Chinese Journal of
POLYMER SCIENCE

REVIEW

https://doi.org/10.1007/s10118-024-3087-7
Chinese J. Polym. Sci. **2024**, *42*, 417–436

Open-Shell Oligomers and Polymers: Theory, Characterization Methods, Molecular Design, and Applications

Xue-Qing Wang, Cheng Song, and Ting Lei*

Key Laboratory of Polymer Chemistry and Physics (Ministry of Education), School of Materials Science and Engineering, Peking University, Beijing 100871, China

Abstract Open-shell oligomers and polymers have exhibited intriguing electronic and magnetic properties, making them highly desirable for a wide range of applications, including ambipolar organic field-effect transistors (OFETs), photodetectors, organic thermoelectrics, and spintronics. Although open-shell ground states have been observed in certain small molecules and doped organic semiconductors, the exploration of open-shell ground-state conjugated polymers is still limited, and the strategies for designing these polymers remain obscure. This review aims to briefly introduce the theory and characterization methods of open-shell conjugated polymers, along with an overview of recent progress and applications. The objective is to stimulate further advancements and investigations in this promising area by shedding light on the potential of open-shell conjugated polymers and the challenges that lie ahead.

Keywords Conjugated polymers; Open-shell molecules; High-spin ground state; Donor-acceptor (D-A) polymers; Optoelectronic and magnetic properties

Citation: Wang, X. Q.; Song, C.; Lei, T. Open-shell oligomers and polymers: theory, characterization methods, molecular design, and applications. *Chinese J. Polym. Sci.* **2024**, *42*, 417–436.

1 INTRODUCTION

Open-shell molecules have unpaired electrons and their total spin quantum number $S = n/2 \geq 1/2$, and n refers to the number of spins. Among them, molecules with $S \geq 1$ are called high-spin ground state molecules. Molecules with high spin have multiple radicals that interact in a way that causes the spins to couple ferromagnetically, resulting in high spin multiplicity.[1] Due to the intriguing electronic and magnetic properties of open-shell molecules, especially high-spin molecules, they have potential applications in electronics and organic magnetism.[2,3] Moreover, due to their light atom composition, open-shell organic molecules have weak spin-orbit coupling and long spin lifetimes, which are critical to the realization of emerging organic spintronics.[4] Open-shell radicals are usually thermodynamically and kinetically unstable due to their incompletely satisfied valency,[5] making the design, synthesis, and purification of these molecules challenging. However, the rapid development of radical chemistry in the past decades has demonstrated the possibility of preparing stable radicals by the use of large steric hindrance groups to protect unpaired electrons and the delocalization of unpaired electrons to large conjugated systems.[5,6] The conventional spin pairing in organic molecules usually has a singlet ground state (S=0), which has an energy gap of tens of kcal·mol^{-1} with the nearest excited triplet state (S=1). The singlet-triplet gap ($\Delta E_{S\text{-}T} = E_{singlet} - E_{triplet}$) is negative (typically<−5 kcal·mol^{-1}), and molecules have a closed shell (S=0). A stable triplet ground state can only be achieved when $\Delta E_{S\text{-}T}$ exceeds 0.6 kcal·mol^{-1} (the thermal energy at room temperature), whereas all the high-spin conjugated polymers reported to date only show a $\Delta E_{S\text{-}T}$ value on the order of 10^{-2} kcal·mol^{-1} to 10^{-3} kcal·mol^{-1}.[7–10]

Open-shell ground states have been observed in some quinoidal small molecules. Open-shell small molecules have already been summarized in several reviews.[1,6,11–13] Open-shell oligomers and polymers offer novel properties and stabilize high-spin ground states on account of their extended π-

* Corresponding author, E-mail: tinglei@pku.edu.cn

Received October 23, 2023; Accepted January 4, 2024; Published online January 25, 2024

delocalization and stronger electronic correlations when compared to small molecular materials, but few studies on the progress of open-shell oligomers and polymers have been published, and most of them focus on the realization of stability, synthetic strategies, and related functions and applications.[14–16] Given the growing interest and fast development of open-shell oligomers and polymers, there is a clear demand for a comprehensive article focusing on the characterization methods, which are important for facilitating a deeper understanding of their magnetic properties. In this review, we first introduce the basic theory of diradicals and polyradicals that constitute open-shell molecules. We then present the computational and experimental characterization methods for open-shell oligomers and polymers, followed by a detailed discussion of open-shell quinoidal π-conjugated molecules, quinoidal-aromatic alternating copolymers, and polymers with polyradicals. Finally, the applications of these high-spin oligomers and polymers in field-effect transistors, photodetectors, thermoelectrics, and spintronics are exemplified.

2 DIRADICAL AND POLYRADICAL

2.1 Diradical

In molecules, the distance (r) between the two radicals and the one-electron overlap integral (S_{AB}) are important factors that influence the ground state properties (Fig. 1a). When the r between two electrons is very large, S_{AB} between the unpaired electrons can be almost neglected. In this case, we can refer to it as a "biradical", not a diradical, where two single radicals coexist in one molecule. When the r between two electrons in a molecule becomes close enough to generate spin-spin interaction between them, we refer to it as a “diradical”. If the separation of the molecular orbitals is sufficiently small, Hund's rule dictates that the triplet state is favored as the ground state. As S_{AB} increases, the two molecular orbitals split, with one orbital becoming bonding and lowered, while the other becomes antibonding and raised. This results in the triplet state being raised, while the system tends to adopt a closed-shell singlet configuration as the ground state, in which the two electrons are paired in the lower orbital. As a result, the nature of the singlet wave function gradually changes from an "open shell" to a "closed shell".[3] A diradicaloid can be described as a system that is intermediate between a diradical and a closed-shell molecule. In this region, the ΔE_{ST} is small, and the singlet state is preferred over the triplet as the ground state (Fig. 1b).

A parameter is needed to describe open-shell diradical species. Theoretically, natural orbital (NO) occupancy was proposed to be a measure of diradical character.[17] In "closed-shell" molecules, the NO occupancies are typically close to two or close to zero, indicating a strongly coupled electron pair or an empty orbital. In a pure diradical, the NO occupancies of the two frontier NOs are close to one, indicating an uncoupled electron pair. However, in the intermediate diradicaloid state, the frontier orbitals can mix due to a small energy gap, resulting in NO occupancies in the lowest unoccupied natural orbitals (LUNOs) ranging from zero to one. This leads to a diradical character y_0, which is always between 0 and 1. y_0 can be formally expressed by Yamaguchi's scheme:[18]

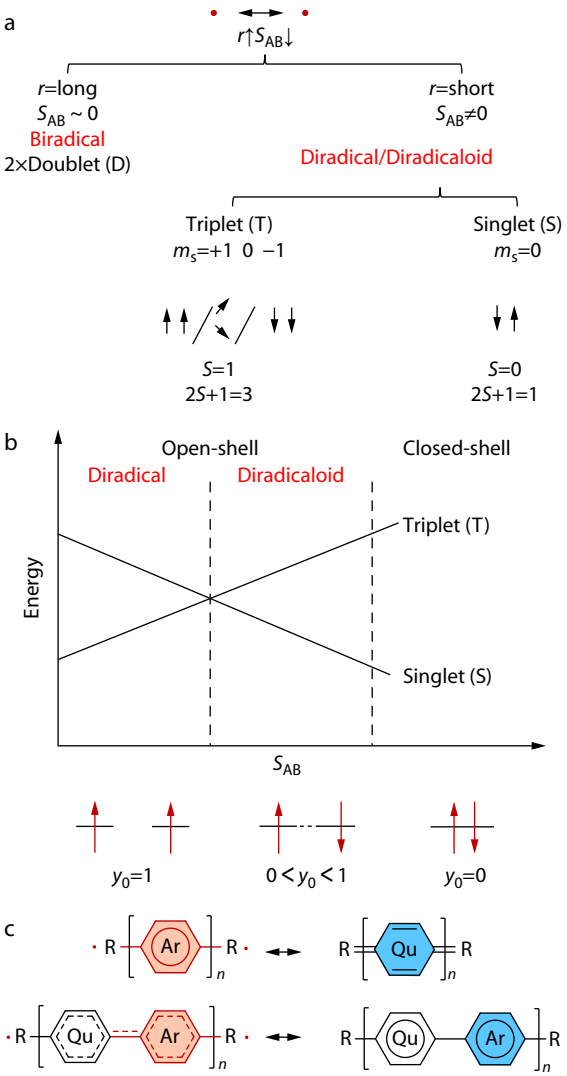

Fig. 1 (a) Electron coupling of biradical and diradical or diradicaloid; (b) Change of the energies of the (triplet, singlet) pair with the increase of the one-electron overlap integral S_{AB}, and the corresponding change of the diradical character (y_0); (c) Aromatic and quinoid transformation of quinoidal conjugated polymers and D-A conjugated polymers with quinoidal acceptor and aromatic donor building blocks.

$$y_0 = 1 - \frac{2T}{1+T^2};\ T = \frac{n_{HONO} - n_{LUNO}}{2} \quad (1)$$

where T is the orbital overlap between the corresponding orbital pairs and can also be represented by using the occupation numbers (n) of the NO.

The majority of conjugated polymers consist of cyclic π-units incorporated into the main chain. These constituent units can be depicted in either a Hückel aromatic or a "quinoidal" form. In the aromatic form, the building blocks exhibit aromaticity within their local rings and are typically interconnected by single bonds. Conversely, in the quinoidal form, a π-unit lacks local ring aromaticity and is commonly linked to others by double bonds. If an aromatic π-conjugated unit demonstrates significant resonance contribution from the quinoidal form, it can also be referred to as "pro-quinoidal".[16]

https://doi.org/10.1007/s10118-024-3087-7

Diradicals can be observed in two typical types of molecules. One type is quinoidal conjugated polymers,[11] The open-shell diradical character in these molecules can be attributed to the increased resonance contribution of the diradical form, which is stabilized by the original quinoidal ring acquiring Hückle aromaticity.[19] The second type is D-A conjugated polymers, which have received more attention in recent years. This type of polymer is typically synthesized *via* cross coupling (Stille or Suzuki coupling) polymerization using pro-quinoidal acceptors and aromatic donors.[16] They exhibit significant quinoidal character due to the presence of quinoidal or pro-quinoidal building accepter blocks. The π system undergoes aromatization resulting in an open-shell ground state. These materials have gained widespread attention and are being extensively researched due to their attractive electrical properties and the availability of mature synthesis methods, but the strategy for achieving a high-spin state with simultaneously desired optoelectronic performance in them by adjusting chemical structure, spin topology, and molecular stacking is still unclear. Detailed examples will be provided in sections **4.1** and **4.2**.

2.2 Polyradical

Polyradical refers to a molecule or compound that contains more than two unpaired electrons. Linear polyradicals can be divided into two types: polymers with spin-containing units in the main chain and those with spin-containing units in the side chains. The first type of polymer exhibits a major weakness. If spin is not generated in some of the spin-containing units, the ferromagnetic interaction is interrupted, and the polymer is divided into several clusters, showing lower multiplicities than theoretically predicted. The second type of polymers are more resistant to spin defects because they undergo magnetic interaction through the conjugated π system (Fig. 2). The design of

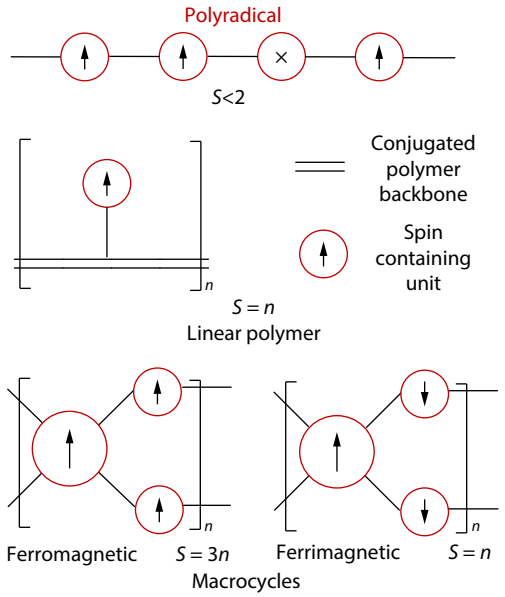

Fig. 2 Description of polyradicals. Models of high-spin linear polymers with spin-containing units in the main chain and those with spin-containing units in the side chains. Models of high-spin macrocycles with the ferromagnetic or antiferromagnetic coupling of polyradicals.

oligomers and polymers consisting of conjugated main chain and pendant groups of free radical nature was first proposed by Ovchinnikov *et al.* (Fig. 2)[20] Ideally, their S is equal to n, but the actual value is often lower than the theoretical value due to the effect of system planarity,[21] the sign of exchange interactions,[22] and the influence of conformational changes.[23]

The challenges encountered in the design and preparation of high-spin linear polymers have been at least partially overcome by using cyclic structures. Cyclic molecules have several advantages compared to linear ones: significantly reducing the impact of spin defects on the total multiplicity of the system, the existence of many spin-coupling paths that can increase ferromagnetic interaction, and the rigid structure of macrocyclic molecules reduces the number of possible conformations, but there is also the problem of antiferromagnetic coupling in circular molecules, which will greatly reduce the S.[24] Detailed examples will be provided in section **4.3**.

3 COMPUTATIONAL STUDIES AND CHARACTERIZATION METHODS

Quantum chemical calculation enables scientists not only to understand the molecular structure and electronic properties of these species but also provides an approach to rationally design new open-shell molecules with new characteristics. Electron paramagnetic resonance (EPR) spectroscopy and superconducting quantum interference device (SQUID) magnetometry are two major techniques utilized to characterize open-shell conjugated polymers.

3.1 Quantum Chemical Calculations

The accurate energy distance between singlet and triplet states is very important for understanding the characteristics of double radicals. The $\Delta E_{S\text{-}T}$ is calculated by the following equation: $\Delta E_{S\text{-}T} = \Delta E_S - \Delta E_T = 2J$. A positive J value indicates the triplet state is more stable and a negative value indicates the singlet state is more stable. Various quantum-chemical calculation methods aiming at accurate prediction of $\Delta E_{S\text{-}T}$ have been developed. Multi-reference *ab initio* methods, such as coupled-cluster singles and doubles with perturbative triples (CCSD (T))[25] and second-order perturbation theory (CASPT2),[26] use multiple slater determinants to provide a more flexible representation of the electronic wave function. These methods are excellent for predicting the reactivity and structures of diradicals, as they can accurately reproduce experimentally determined $\Delta E_{S\text{-}T}$.[3] However, the computational cost of these methods is quite high, making it difficult to apply them to conjugated polymers. Density functional theory (DFT)[27] greatly reduces the computational cost. The triplet states can generally be calculated accurately by methods with conventional unrestricted wave functions such as unrestricted density functional theory (UDFT). However, it cannot accurately describe the electronic configuration of open-shell singlet states, resulting in significant uncertainty in $\Delta E_{S\text{-}T}$ computation. The broken symmetry (BS) formalism proposed by Noodleman and Yamaguchi is a possible compromise method that accurately describes singlet diradicals and is now widely used in the computational study of conjugated polymers.[28,29] The BS solution is not the pure eigenstate of the singlet double radicals, but the mixed state of the singlet state and the triplet state. To provide a reliable $\Delta E_{S\text{-}T}$,

singlet energy values need to be improved, Yamaguchi and colleagues[30] developed a spin correction (SC) method to eliminate spin pollution. Spin pollution can be determined based on the calculated value of $\langle S_2 \rangle = \langle S(s+1) \rangle$. For the pure triplet state, the value of $\langle S_2 \rangle_T$ is 2, while the value of $\langle S_2 \rangle_{BS}$ for the pure singlet state is 1. Therefore, when the $\langle S_2 \rangle_{BS}$ value is less than 1, the contribution of the closed shell electronic configuration is included in the singlet state. When the $\langle S_2 \rangle_{BS}$ value is higher than 1, it indicates that there is triplet-state pollution in the singlet state. Kitagawa and colleagues[31] recently developed an approximate spin projection (AP) method to enhance computational accuracy by minimizing the remaining spin contamination in the singlet energy. Nakano *et al.*[32] used the approximate spin-projected spin-unrestricted density functional theory with long-range correction, approximate spin-projected (ASP) long-range corrected (LC) UBLYP, and obtained the approximate results with the unrestricted coupled-cluster singles and doubles with perturbative triples (UCCSD (T)) method.

$$\Delta E_{S-T}^{SC} = E_S^{SC} - E_T = \Delta E_{S-T} \frac{\langle S^2 \rangle_T}{2(\langle S^2 \rangle_T - \langle S^2 \rangle_{BS})} \quad (2)$$

The commonly used DFT functional B3LYP only contains 20% Hartree-Fock (HF) exchange, and the calculated *y*-value is significantly lower than *ab initio* calculations. Thomas *et al.*[33] found BHandHLYP that containing 50% HF can better reproduce the diradical character y_0 and reduce overestimation of the delocalization of the conjugated system, but it is easy to show wave function instability. Meanwhile, the LC-UBLYP and coulomb attenuating method (CAM) UB3LYP methods are found to be very suitable for evaluating the biradical characteristics of open-shell singlet systems.[34] LC-UBLYP was found to give structures in close agreement with those calculated by *ab initio* calculations. However, Sabuj *et al.*[35] compared the functions of different HF exchange quantities and found that B3LYP has the lowest spin pollution among all considered mixed-density functional theories. Other functional functions can generate significant spin pollution, leading to an increase in the characteristics of double radicals and even nonphysical polyradicals.

In addition to the direct calculation of biradical properties, the calculation of aromatic properties is also an important means to study open-shell conjugated polymers. The aromatic and quinoidal properties of molecules can be studied by bond length alternation (BLA) analysis and Nucleus-Independent Chemical Shift (NICS) calculations. In compounds containing quinoidal structures, the sharing of conjugated π electrons and the dispersion of electron clouds lead to a minimal difference in bond lengths between adjacent bonds. This is due to the uniform distribution of electron density within the conjugated system, resulting in closely matched electron densities for neighboring bonds and consequently minimal BLA. NICS values can be used to determine whether a molecule exhibits aromaticity in its cyclic π-electron system. The negative NICS values represent aromaticity, the positive NICS values represent antiaromaticity, and the NICS values close to 0 indicate non-aromaticity.

Azoulay *et al.*[7] recently reported a novel conjugated polymer (**P1**) comprising alternating benzo[1,2-b:4,5-*b*′]dithiophene donor units and a newly developed 6,7,8,9-tetrachloro-[1,2,5]thiadiazolo[3,4-*b*]phenazine acceptor with strong electron-withdrawing properties. Their study included a comparative analysis with a 6,7-dimethyl-[1,2,5]thiadiazolo[3,4-*g*]quinoxaline (TQ) acceptor (the acceptor in **P2**). They showed that the incorporation of annulation and chlorination into the TQ framework facilitated a transition from closed-shell aromatic to high-spin quinoidal forms (Fig. 3a). BLA between the donor and acceptor units of the **P1** and **P2** are calculated. **P1** with diradical properties has a significantly smaller BLA compared to **P2** with a closed shell. BLA of **P1** reveals a quinoidal-to-aromatic transition emanating from the center of the chain, with the shortest bonds of 1.413 Å (bond 7) and 1.413 Å (bond 8) localized to a single central acceptor unit. This delocalized bonding transition ultimately requires longer conjugation lengths for configuration mixing to stabilize the quinoidal bonding pattern along the π-conjugated backbone (Fig. 3b). $NICS_{zz}$ was computed by the gauge independent atomic orbital (GIAO) method on the BS optimized geometry by single point energy calculation at the UB3LYP/6-31G** level of theory at 1 Å perpendicular to the ring plane to account for only the π electron contribution. At this distance, the contribution of the π-electrons is maximized. The **P2** exhibited a greater degree of aromaticity, as evidenced by a more negative NICS value of its benzenoid rings in the acceptor, whereas **P1** underwent a quinone transformation, resulting in a high NICS value, and showed a high NICS value of 0.86 (Fig. 3c, Ring 4A). The modulation of the spin density distribution controls the electronic and magnetic properties of the ground state. Rai *et al.*[10] introduced two D-A conjugated polymers that combine cyclopentadithiophene (CPDT) donors with benzobisthiadiazole (BBT) and iso-BBT acceptors, compared with the previously reported CPDT-TQ system (Fig. 4a). CPDT-TQ exhibits a high-spin ground state, characterized by a delocalized spin density distribution throughout the entire chain. DFT calculations reveal that the CPDT-BBT system exhibits a significant separation between the unpaired electrons, resulting in a pure diradical nature, hampers the covalency of π-bonds and confines the unpaired spins to the ends of the polymer. Conversely, substituting the BBT acceptor with iso-BBT produces a closed-shell configuration characterized by a low-spin ground state and localized spin density within the polymer cores (Fig. 4b). Therefore, it seems that the closed-shell materials with a low-spin ground state tend to accumulate the spin density in the middle of the molecular backbone, whereas the open-shell materials with a high-spin ground-state show either a delocalized or an end-localized orbital topology.[35,36] Similar patterns have also been observed in molecules reported by other researchers.[7,8,37]

3.2 EPR

Continuous-wave electron paramagnetic resonance (CW-EPR)[38,39] is an effective method for studying open-shell polymers, as it selectively detects paramagnetic components of the sample with high sensitivity. In a CW experiment, low-intensity monochromatic microwave radiation is continuously applied to the sample. By sweeping the magnetic field over a specific range, the applied microwave radiation brings different EPR transitions into resonance. Triplet states are the only EPR-active species in diradicals. The Zeeman effect does not apply for singlet diradicals, because the spin quantum number of singlet states is zero. Triplet states have three corresponding triplet sublevels X, Y, and Z in zero fields, the energies of the triplet sublevels are usually non-degenerate and the relative splittings

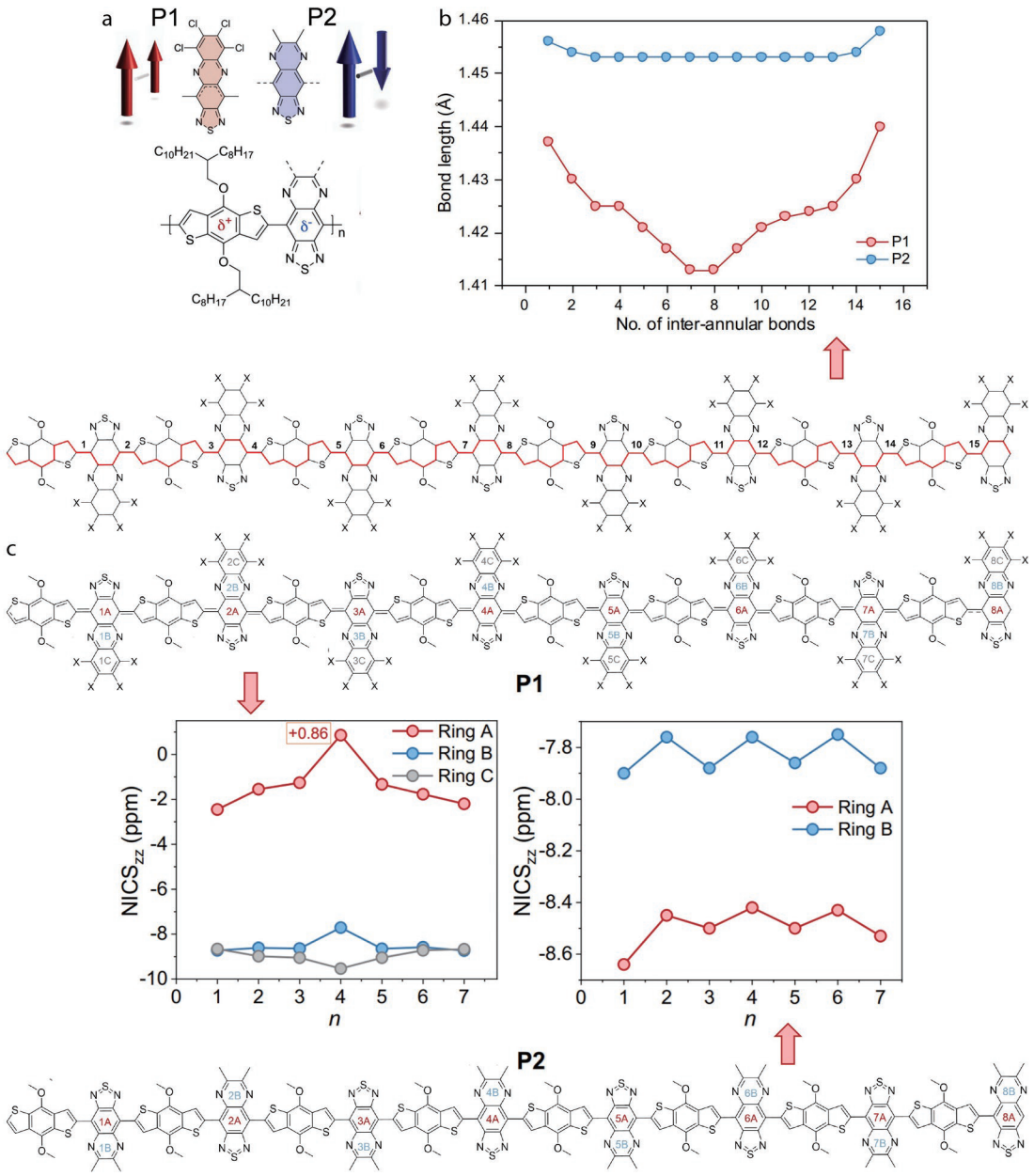

Fig. 3 (a) Chemical structures of **P1** and **P2**, (b) BLA between the donor and acceptor units of **P1** and **P2** upon π-extension. (c) NICS values are computed for rings 'A', 'B', and 'C' of the octamers of **P1** and **P2** which exhibit aromatic and quinoidal (anti-aromatic) characteristics at the DFT/UB3LYP/6-31G** level. (Reproduced with permission from Ref. [7]; Copyright (2023), American Chemical Society.)

depend on the zero-field splitting (ZFS) parameters, as sketched in Fig. 4(a). The relative energies of the three levels are described by two ZFS parameters: D and E. When an external field is applied as customary in EPR, the electron Zeeman interaction needs to be considered. When the applied magnetic field is parallel to the Z sublevel, the triplet sublevels are labeled as 0, +1 and −1 (Fig. 5a). The EPR spectrum features two allowed (Δm_s=±1) transitions for each molecular orientation (Fig. 5a). Since the sublevels are spin polarised, both enhanced absorption and emission peaks are observed (Fig. 5b). When the sample is isotropic and all possible orientations are present (*i.e.*, in a powder sample or frozen solution), the resulting powder average spectrum (Fig. 5c) has six distinguishable turning points. From their positions, the magnitude of the ZFS parameters can be derived. If E=0 (*i.e.*, X = Y) only four turning points are present.

The EPR signal intensity (I) could exhibit temperature (T) dependence. The EPR signal of doublet state species shows a linear relationship with temperature. As the temperature decreases, the EPR intensity of the triplet state deviates upward from the linear fitting, while the singlet state is opposite (Fig. 5d). $\Delta E_{S\text{-}T}$ can be determined by fitting the data using the Bleaney-Bowers equation:[40]

$$I = C\left[\frac{3\exp(-2J_{ab}/kT)}{1+3\exp(-2J_{ab}/kT)}\right]\frac{1}{T} \quad (3)$$

where C is the Curie constant, J_{ab} is the exchange integral, J_{ab}<0 (singlet ground state), and J_{ab}>0 (triplet ground state). For sin-

https://doi.org/10.1007/s10118-024-3087-7

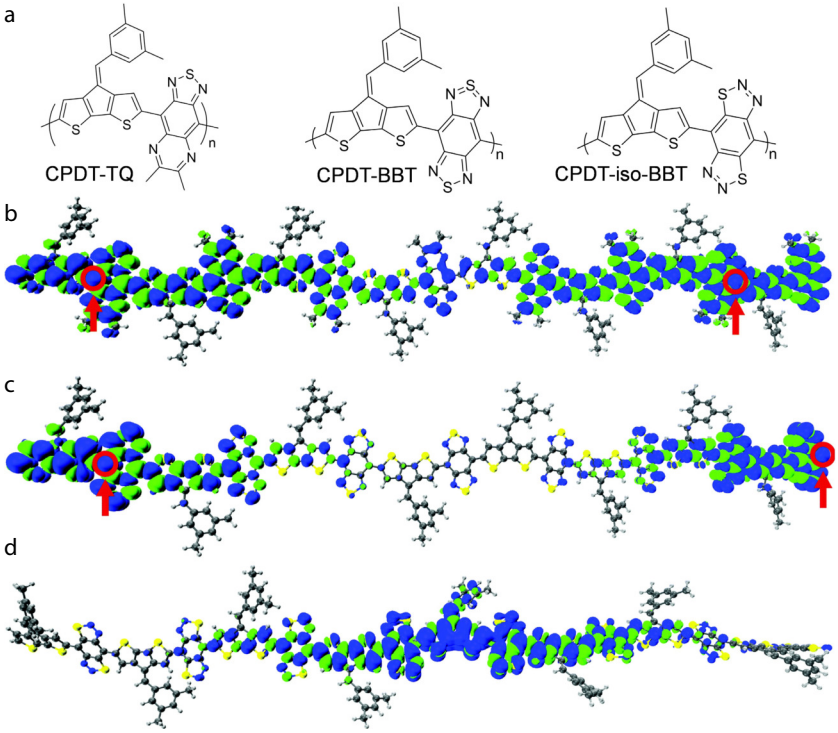

Fig. 4 (a) Chemical structures of CPDT-TQ, CPDT-BBT and CPDT-iso-BBT. The ground-state geometry and pictorial representations of the spin density distribution of the (b) CPDT-TQ, (c) CPDT-BBT, and (d) CPDT-iso-BBT. (Reproduced with permission from Ref. [35]; Copyright (2021), the Royal Society of Chemistry.)

glet-ground-state diradicals, this equation can be utilized to determine singlet-triplet energy gaps of less than 1 kcal·mol^{-1}, making it applicable for highly reactive diradicals. In the case of triplet-ground-state molecules, this equation is particularly useful when the energy gap is below 0.1 kcal·mol^{-1}.[3]

Taking polymer p(TDPP-BBT) developed by Lei *et al.* as an example,[8] in the presence of electron spins with a multiplicity of S=1 (triplet ground state), the CW-EPR spectra exhibit two characteristic features: (i) fine structure resulting from electron-electron interactions, specifically the ZFS interaction which dominates the EPR spectrum, and (ii) a weaker additional signal observed at half-field due to the forbidden $|\Delta m_s|$=2 EPR transition (Fig. 6b). Furthermore, the variable temperature EPR of p(TDPP-BBT) in solution was also measured and showed a similar behavior compared to solid state EPR. The EPR intensities decrease with the increase of temperature (Fig. 6c). The EPR data of p(TDPP-BBT) from 4.9 K to 50 K were fitted by Eq. (3) (Fig. 6d), giving a positive $\Delta E_{S\text{-}T}$ of 4.92×10^{-3} kcal·mol^{-1} (corresponding to J=2.48 K), suggesting the polymer has a triplet ground state.

3.3 SQUID

SQUID[41,42] is the most popular technique to study the magnetic properties of open-shell polymers. Direct-current (DC) SQUID can measure the bulk magnetic response properties that are not available using EPR, which includes temperature-dependent majority spin alignment, magnetic phase transitions, diamagnetic susceptibility, morphological dependencies, and their relative contributions to the magnetic features. However, compared with EPR, the SQUID requires a large amount of samples (10–100 mg), and SQUID measures the paramagnetic signal and diamagnetic signal at the same time, so the diamagnetic signal needs to be deducted. The low-temperature DC-SQUID is composed of two Josephson junctions. Because of the macroscopic quantum interference effect, the voltage at both ends of the tunnel junction is a periodic function of the change of the external magnetic flux in the input loop. The input loop is connected to a much larger pickup loop, which can greatly increase the effective area and improve the sensitivity of SQUID. In the detection of weak magnetic signals, the background field is often several orders of magnitude larger than the signal. In this case, the second-order gradiometer is particularly useful, which can distinguish the far-field noise from the near-field signal (Fig. 7a). In the DC mode, the sample position moves from top to bottom through the space gradiometer, producing a voltage waveform. The magnetic moment of the sample is obtained after fitting the voltage signal. In the vibrating sample magnetometry (VSM) mode, the sample oscillates within a much smaller region of the gradiometer, producing a simpler response (Fig. 7b). The accuracy of the DC mode reaches the order of 5×10^{8} emu. Combining VSM and SQUID can further improve the measurement accuracy by at least 5 times, with the accuracy of less than 1×10^{-8} emu. The above two modes can be operated automatically to measure sample magnetization as a function of magnetic field and temperature.

The sample must be handled with care to avoid any type of magnetic contamination. The background signal is always significant and must be carefully removed. The presence of background signals from the sample holder can effectively obscure weak magnetic moment signals. Therefore, it is crucial to take into account the characteristics of the sample holder. Thus, aluminium capsules are widely utilized due to their low intrinsic magnetic moment; however, defect-

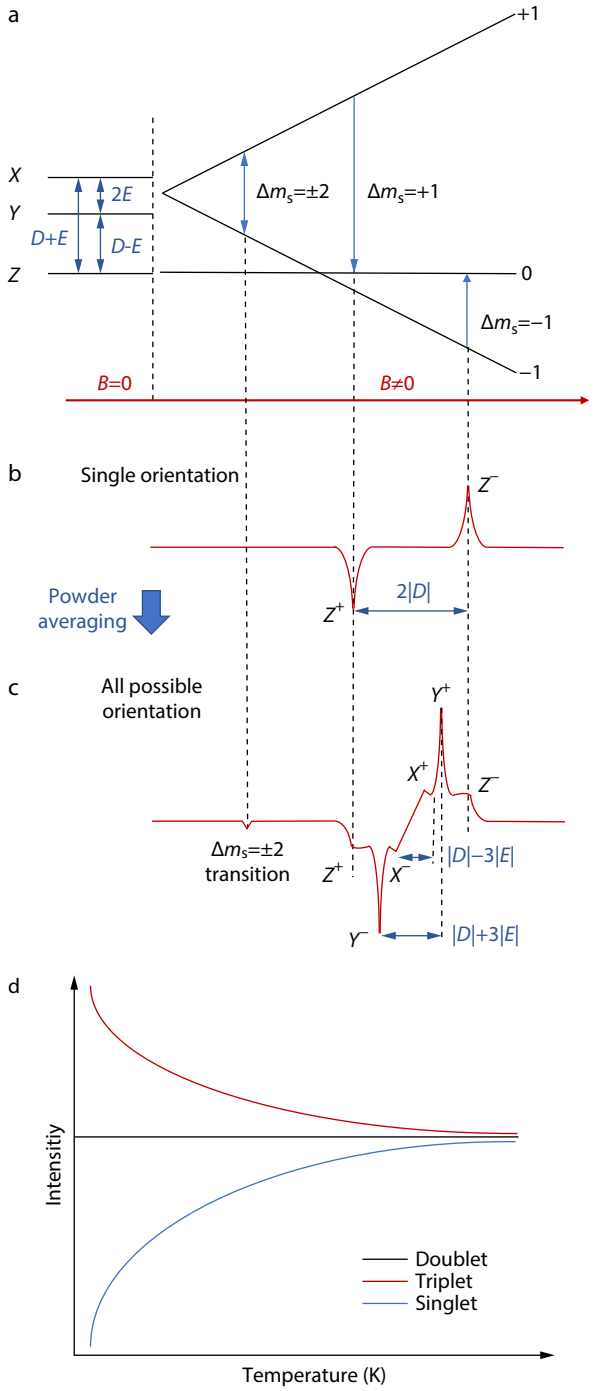

Fig. 5 Typical EPR spectra of triplet diradicals in the solid state. (a) ZFS and the electron Zeeman interaction when an external field is applied; EPR signal of (b) single orientation sample and (c) all possible orientation sample; (d) Ideally, typical temperature dependent changes of EPR signal intensities for triplet, doublet, and singlet ground-state radicals.

induced magnetic responses can occur from bending or creasing.

Due to several factors, such as spin pairing, π-conjugation, and the presence of light elements, the magnetic moment of organic materials is relatively low, making the negligible diamagnetic effect in most organic materials indispensable or even significant. To accurately analyse the magnetic properties of such materials, Pascal's corrections should be applied to the data to theoretically eliminate the intrinsic diamagnetic contribution.[43] Closed-shell singlets typically exhibit a large $|\Delta E_{S\text{-}T}|$, resulting in unremarkable and predominantly diamagnetic magnetometry behavior. Narrow-bandgap open-shell conjugated polymers often possess a small $|\Delta E_{S\text{-}T}|$, allowing the first spin-excited state to be thermally populated. This thermally accessible triplet state can be detected by measuring the magnetic moment as a function of temperature. Therefore, a singlet diradical with a thermally accessible triplet state exhibits a noticeable diamagnetic-to-paramagnetic transition as the temperature increases and the triplet manifold becomes populated. On the other hand, triplet diradicals display a paramagnetic signal at low temperatures. The magnetic properties of these systems can be quantified by fitting experimental data to Curie-Weiss equations used for ideal paramagnets.

The temperature-dependent χ has been widely used to determine the magnetic phase and thermally induced magnetic property changes.[44] The relationship between χ and T can be described by Curie Weiss law:[45]

$$\chi = \frac{C}{T-\theta} + \chi_0 \quad (4)$$

where χ is the magnetic susceptibility, C is the Curie constant, T is the temperature, θ is the Curie temperature and χ_0 is a vertical offset that accounts for any observable diamagnetism. The Curie temperature determines the magnetic behaviour of a material. When θ is positive, it indicates that the material exhibits paramagnetism, whereas a negative θ indicates diamagnetism. The Curie-Weiss law is applicable when the temperature is significantly lower than the Curie temperature and remains valid within a specific temperature range.

Fig. 7(c) shows the temperature dependence of the processed voltage of a high-spin polymer (**14**) in a constant magnetic field of 1 T over a temperature range of 2 K to 400 K. Fig. 7(d) illustrates the corresponding magnetic susceptibility (χ). As the temperature increases, the magnetic moment decreases rapidly, following a Curie-like behavior.[37] More information can be obtained by comparing the temperature dependent magnetic susceptibility of ZFC and FC. If the ZFC and FC curves completely coincide, it indicates paramagnetic behaviour. A slight difference suggests possible magnetic phenomena or variations in the magnetic field. Azoulay *et al.*[46] compared the temperature dependence of magnetic susceptibility between amorphous solid powders of high-spin polymers (**17**) and solvent vapor assisted ordered films. The former almost overlaps, while the latter has some splitting (Figs. 8a and 8d), the former exhibits paramagnetism and is largely isotropic, while the latter exhibits highly anisotropic spin ordering and exchange interactions. The significant upward shift of χ in the latter suggests the presence of a large amount of delocalized Pauli-type carriers. The amorphous materials show a small θ of –1.1 K for the FC curve and –0.39 K for the ZFC curve according to Curie-Weiss law (Eq. 4), suggesting short-range antiferromagnetic interactions between small populations of unpaired electron spins.

The determination of the spin multiplicity S of the magnetic ground state involves measuring the magnetization as a function of the magnetic field at low temperatures, ensuring

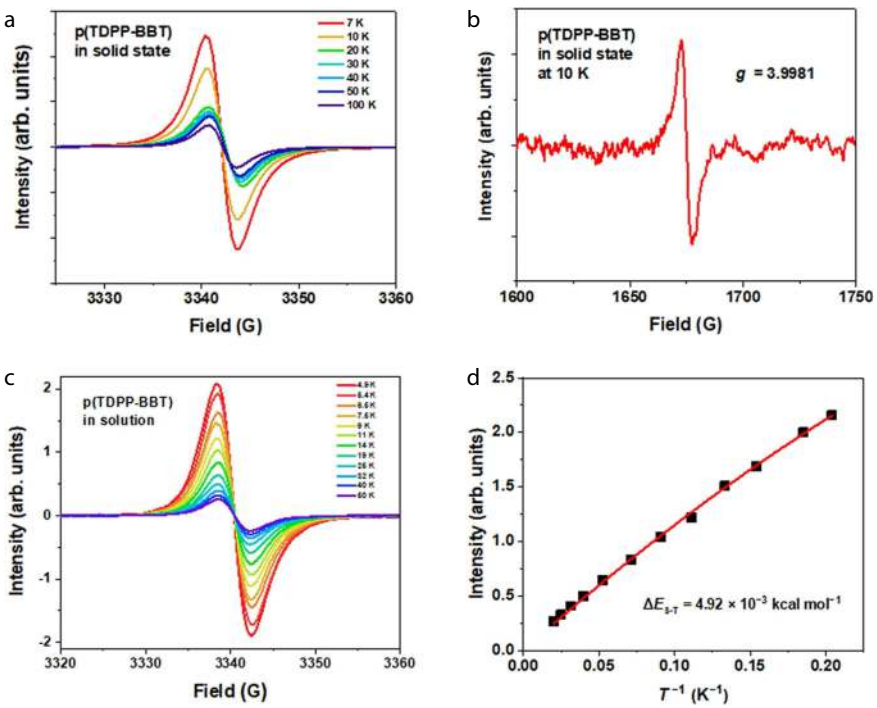

Fig. 6 CW-EPR experiments of polymer p(TDPP-BBT), which has a triplet ground state. (a) Variable temperature EPR of p(TDPP-BBT) in the solid state; (b) The half-field line of p(TDPP-BBT) in the solid state: $|\Delta m_s| = 2$; (c) Temperature-dependent EPR of p(TDPP-BBT) in a 1×10^{-5} mol/L *o*-xylene solution; (d) The corresponding Bleaney-Bowers equation fitting result for Fig. 5(c). (Reproduced with permission from Ref. [8]; Copyright (2022) from Nature.)

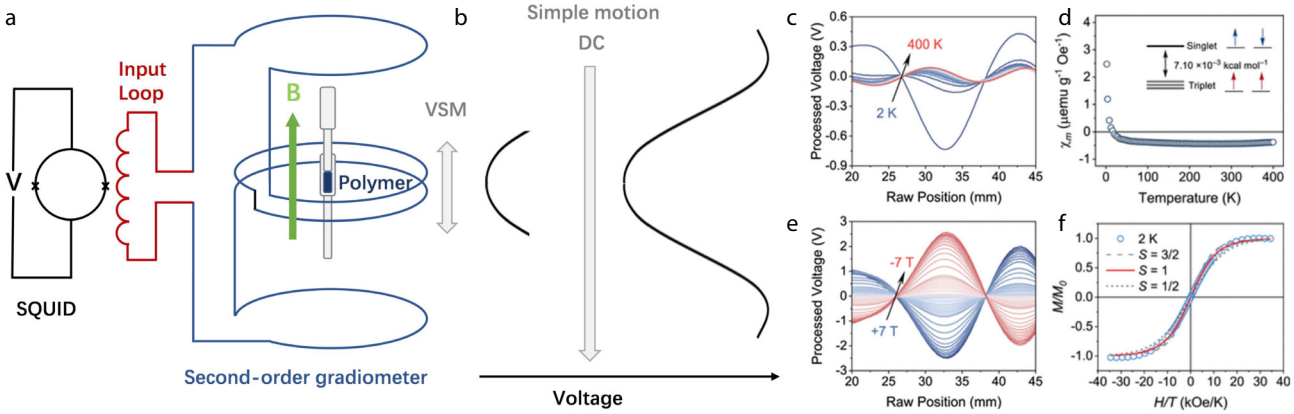

Fig. 7 (a) Schematic illustration of magnetometry measurement of a polymer sample within a capsule; (b) In the DC mode (right), the sample moves through the length of the gradiometer, producing a voltage waveform in response to an applied magnetic field *B*. In the VSM mode (left), the sample oscillates within a much smaller region of the gradiometer, producing a simpler response; (c) Processed voltage versus raw sample position with varying temperature and a constant magnetic field *H* of 1 T; (d) χ_m versus *T*, generated automatically from voltage measurements shown in part (c), with associated $\Delta E_{S\text{-}T}$; (e) Processed voltage versus raw sample position with a varying magnetic field and a constant temperature of 2 K; (f) Normalized magnetization versus *H*/*T*, generated automatically from voltage measurements shown in part (e), The best representation of the data is achieved with *S*=1. (Reproduced with permission from Ref. [37]; Copyright (2022), American Chemical Society.)

that only the magnetic ground state is populated. In the case of a sample containing a high-spin polymer with a single spin state of a specific multiplicity, the measured data can be directly correlated to *S* by comparing the experimental curve with the expected paramagnetic Brillouin function[47] (Eq. 5) curves corresponding to different *S* values.

$$M = M_0\left[\frac{2S+1}{2S}\coth\left(\frac{2S+1}{2S}\frac{gS\mu H}{kT}\right) - \frac{1}{2S}\coth\left(\frac{1}{2S}\frac{gS\mu H}{kT}\right)\right] \quad (5)$$

where *g* is the electron *g*-factor, μ is the Bohr magneton, *k* is the Boltzmann constant, *T* is the temperature, M_0 is the saturation magnetization, and *S*, the fitting parameter, is the spin quantum number. The field dependence of the magnetic moment was usually measured in the DC mode for a range of fields at a constant temperature. Fig. 7(e) displays the position dependence of the processed voltage, and Fig. 7(f) shows the corresponding magnetic moment. The data has been corrected for background and diamagnetic effects, and normalized to the saturation magnetization M_0. For comparison, the Brillouin func-

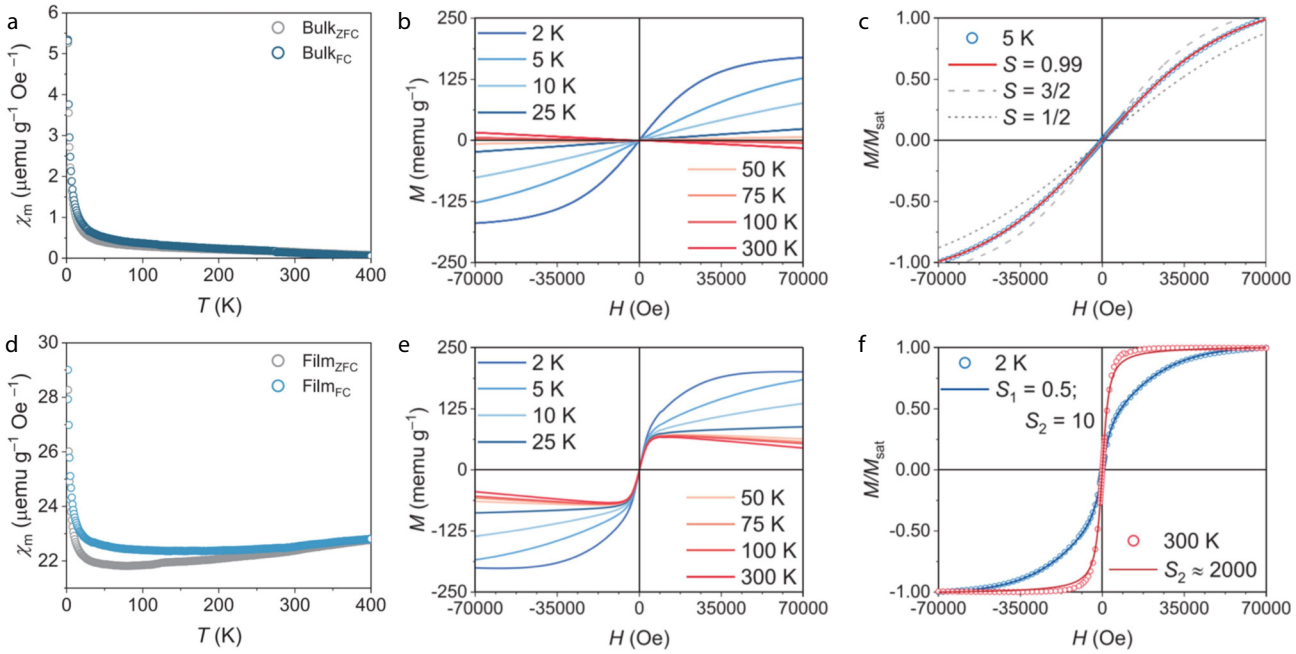

Fig. 8 Zero field cooling (ZFC) and field cooling (FC) susceptibility curves measured for (a) the amorphous and (d) the slow-dried film of a high-spin polymer in the temperature range of 2–400 K. Magnetization curves of (b) the amorphous powder and (e) the slow-dried film sample as a function of the field in the temperature range of 2–300 K, with a field range of −7 T to 7 T. Normalized magnetization curve of (c) the amorphous powder at 2 K. The curve was fitted using the Brillouin function, giving an S=0.99. (f) Normalized magnetization curve of the slow dried film sample at 2 and 300 K. Both curves were fitted to the linear combination of the regular Brillouin function with two S parameters. S_1=0.5, S_2=10, and S_2=2000, for 2 and 300 K, respectively. S_1 has an insignificant contribution to the total spin as compared to S_2 for 300 K. (Reproduced with permission from Ref. [46]; Copyright (2022), Wiley Online Library.)

tion with S=1 provides the closest fit to the experimental data. For a sample bearing a mix of spin states (Fig. 9f). For highly spin-conjugated polymers (**17**), disordered powders can also be well fitted using the Brillouin function, and the best results are obtained at S=0.99 (Fig. 8c). When ordered high-spin aggregates lead to anisotropic spin alignment, the paramagnetic Brillouin function cannot fit them accurately, so the authors employed a linear combination of Brillouin functions (Eq. 6):[48]

$$M = M_1\left[\frac{2S_1+1}{2S_1}\coth\left(\frac{2S_1+1}{2S_1}\frac{gS_1\mu H}{kT}\right)-\frac{1}{2S_1}\coth\left(\frac{1}{2S_1}\frac{gS_1\mu H}{kT}\right)\right]+ M_2\left[\frac{2S_2+1}{2S_2}\coth\left(\frac{2S_2+1}{2S_2}\frac{gS_2\mu H}{kT}\right)-\frac{1}{2S_2}\coth\left(\frac{1}{2S_2}\frac{gS_2\mu H}{kT}\right)\right] \quad (6)$$

where the constants M_1 and M_2 are the saturation moments and S_1 and S_2 are the spin quantum numbers of the Curie like and the high-spin phases, respectively. It provided a better fit to data compared to a single function. The net spin of S_1 shows a moderate increase from approximately 0.7 to 2 as the temperature is varied from 2 K to 50 K. In contrast, S_2 exhibits a more significant increase, ranging from 10 to 290 over the same temperature range. At 100 and 300 K, the S_2 value reached approximately 600 and 2000, respectively (Fig. 8f). Molecular design of high-spin polymers.

4 OPEN-SHELL OLIGOMERS AND POLYMERS

4.1 Quinoidal Type

Given the nascent stage of research on open-shell quinone conjugated oligomers and polymers, there are currently limited examples exhibiting high-spin ground triplet states. Some oligomers or polymers have been able to display thermally accessible triplet states.

Most polymers adhere to the design concept of conjugated small molecules.[49] In 1904 and 1907, scientists successfully synthesized Thiele hydrocarbons[50] and Chichibabin hydrocarbons[51] with *para*-quinodimethanes (p-QDMs) structures (**1** and **2**). These oligomers exhibit resonance structures of both closed-shell quinoid and open-shell aromatic diradicals. To enhance electronic delocalization and molecular stability, researchers introduced electron-withdrawing units into the conjugated structure of p-QDMs. By incorporating cyano groups at the highly active methylene positions, they obtained highly stable tetracyanoquinodimethane (TCNQ, **3**).[52] Further modification with benzene rings in the conjugated backbone led to the formation of tetracyano-dinaphthoquinodimethane (TCNDQ, **4**),[53] but neither of them exhibited a triplet ground state. Compared to TCNQ, TCNDQ exhibited greater aromatic resonance energy, resulting in stronger open-shell diradical characteristics. Wu *et al.*[54] developed a series of quinoid naphthalene-fused molecules with nitrogen rings and cyano end groups, denoted as *n*Per-CN (**5a**–**5f**). The molecular properties varied with the number of repeating units. When n=2–4, strong exchange interaction between the terminal electron and the central naphthalene-fused unit resulted in an open-shell singlet ground state. For n=5–6, molecular twisting due to steric hindrance weakened intramolecular interactions and bonding, leading to an open-shell triplet ground state in **5e** and **5f**. The conclusions were drawn from magnetic susceptibility measurements and tempera-

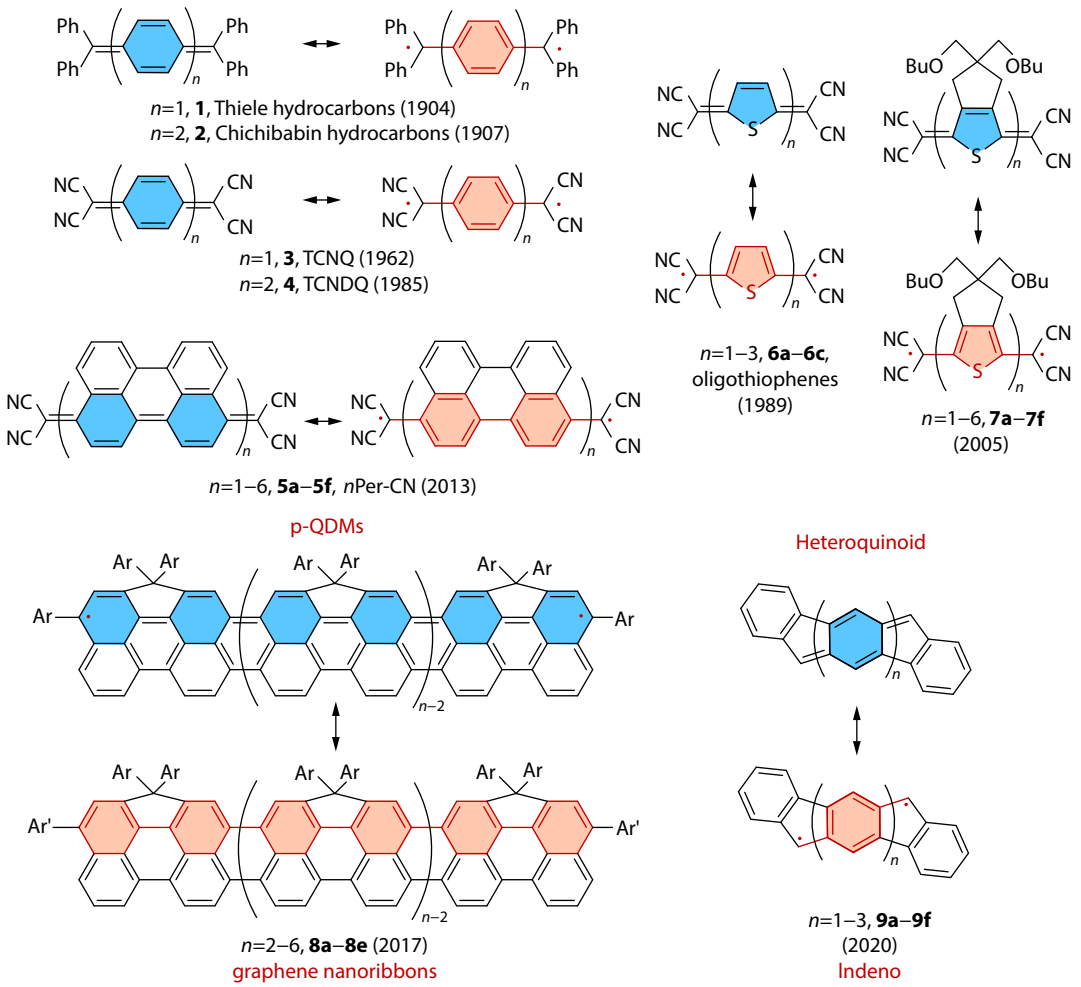

Fig. 9 Quinone-based oligomers and polymers derived from p-QDMs, Heteroquioids, indeno, and graphene nanoribbons exhibiting triplet ground states or thermally accessible triplet states.

ture-dependent EPR spectroscopy. The diradical characteristics have also been observed in oligothiophenes (**6a**–**6c**) with thiophene units replacing benzene units.[55] However, the low solubility hinders further synthesis of moleculars with higher molecular weights. Oligothiophenes (**7a**–**7f**) fused with bis(butoxymethyl)cyclopentane were synthesized.[56] Raman spectroscopy studies revealed thermal equilibrium between singlet and triplet ground states at room temperature for *n*=6.[57] Unlike zigzag-edged graphene nanoribbons (GNRs), where unpaired electrons are primarily localized at the zigzag edges,[58] narrow graphene nanoribbons (**8a**–**8e**) molecules exhibit spin density distribution at both ends and gradually delocalize over the entire backbone as the length increases, which display an uncommon open-shell singlet ground state and paramagnetic properties at room temperature.[59] Indeno[60] is also a common building block for open-shell small molecules, and researchers have observed that extending the conjugation length of the molecule **(9a**–**9f)** can effectively reduce the $\Delta E_{S\text{-}T}$.[43,61]

4.2 Quinoidal-aromatic Alternating Copolymers

Most of the reported quinoidal conjugated oligomers or polymers have inherent limitations. For instance, in the case of polycyclic aromatic hydrocarbons, their synthesis is complicated, and they exhibit poor stability of radicals with low solubility, not good for solution processing.

Recently, many high-spin polymers based on quinoidal-aromatic alternating structures have been designed and synthesized. These polymers have shown interesting high-spin properties. First, their aromatization of the π-system leads to an open-shell ground state. Second, the large effective π-conjugation length allows for extensive delocalization of radicals, leading to higher stability. Third, these polymers exhibit excellent solubility and solution processability, making them suitable for easy fabrication of thin film optoelectronic or spin-electronic devices. Moreover, they have high charge carrier mobilities, as well as well-established synthetic strategies, facilitating their rapid development. Many of these polymers are donor-acceptor (D-A) polymers and have narrow bandgap (0.1 eV<E_g<1 eV), which promote the mixing of frontier molecular orbitals (Fig. 10a).[62,64]

In 2011 and 2015, Bhanuprakash *et al.*[33] and Wudl *et al.*[66] reported the shell opening characteristics of narrow band gap D-A small molecules and polymers based on benzo [1,2-*c*;4,5-*c*]bis[1,2,5] thiadiazole(BBT). Wu *et al.*[63] also observed the biradical characteristics of oligomers based on BBT through experimental and theoretical evidence. At the same time, they

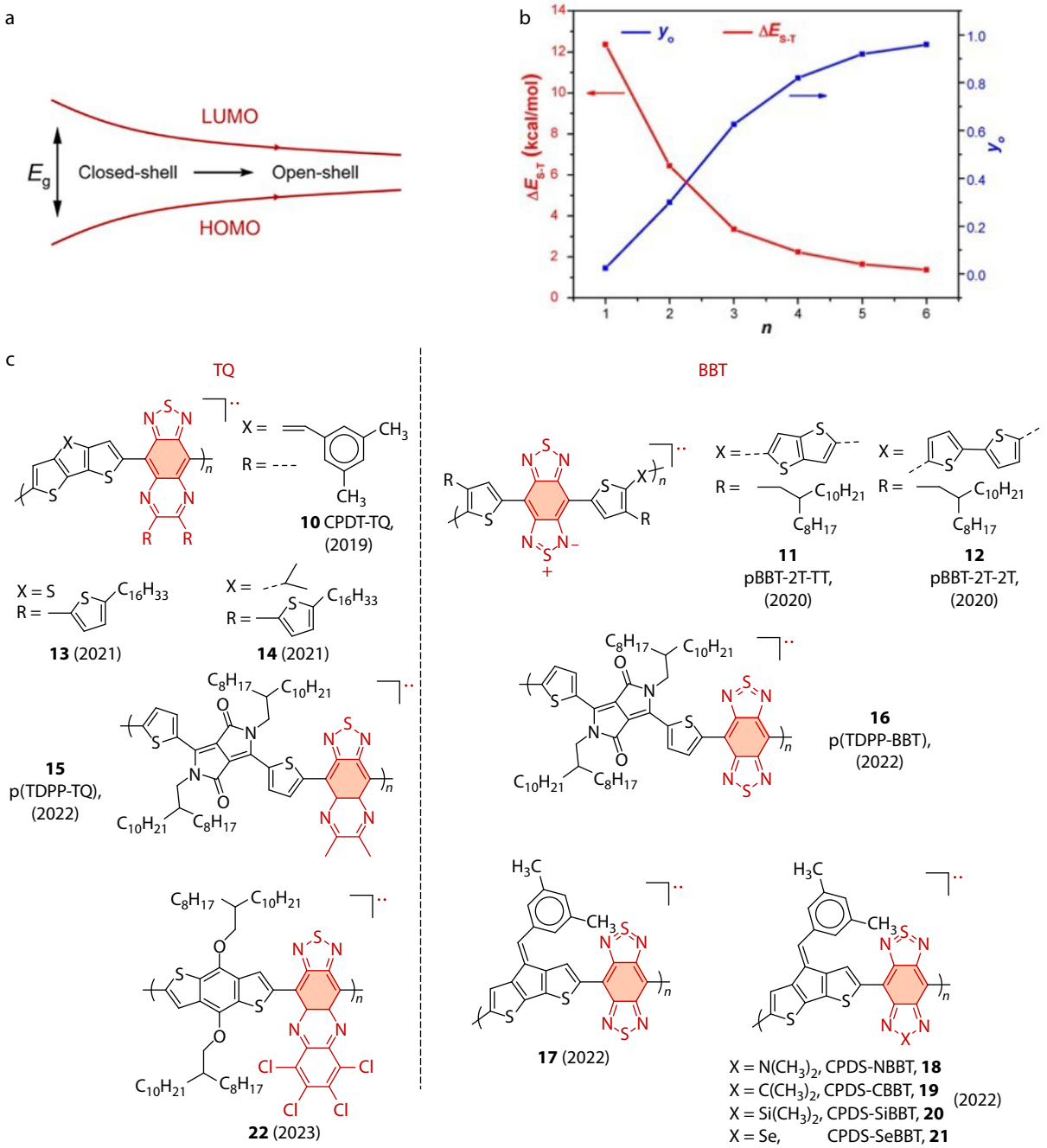

Fig. 10 (a) The narrowing of the bandgap promotes the transition from closed shell to open shell. (Reproduced with permission from Ref. [62]; Copyright (2021), American Chemical Society.) (b) The relationship between the length of π-conjugation and $\Delta E_{S\text{-}T}$. (Reproduced with permission from Ref. [63]; Copyright (2017), Wiley Online Library.) (c) High-spin D-A conjugated polymers. quinone-type receptors can be divided into two categories: TQ and its derivatives and BBT and its derivatives. The serial numbers in the figure are sorted by time.

found that by increasing the length of π-conjugation or introducing electron donor groups at the end, $\Delta E_{S\text{-}T}$ decreases, and the biradical property increases (Fig. 10b). The above work has laid a foundation for the systematic study of high-spin D-A conjugated polymers.

Quinoidal-aromatic copolymers with different polymer building blocks were synthesized, and their design strategies were intensively explored recently. Azoulay *et al.*[10] first proposed the concept of the high-spin ground state D-A conjugated polymer, using alternating CPDT and TQ (**10**). EPR and magnetic susceptibility measurements show that the polymer has a $\Delta E_{S\text{-}T}$ of 9.30×10^{-3} kcal·mol^{-1}. Xu *et al.*[65] found that the antiferromagnetic coupling strength can be controlled by tuning π-π distance. The coupling constant of antiferromagnetic coupling J_{AFM} (kcal per mole repeating unit) is calculated to be −0.55 for TT (**11**) and −0.63 for 2T (**12**), the π-π distances of TT and 2T are 3.51 and 3.45 Å, respectively. These data support the hypothesis that smaller π-π distances lead to

larger $|J_{AFM}|$ (Figs. 11a and 11b).[65] Based on structure **10**, Azoulay *et al.* continued to explore the influence of polymer structure[7,9] on spin topology. By substituting sulfur (**13**) with carbon (**14**) at the donor bridgehead, the local aromaticity in the donor can be adjusted, thus controlling the topology and ground state structure.[9] Lei *et al.*[8] first proposed a computational strategy to rationally screen potential polymer building blocks for designing high-spin ground state and high mobility semiconducting polymers. Based on the strategy, three quinoidal-aromatic copolymers with different spin ground states were obtained. Unlike the above D-A polymers, these polymers are based on acceptor-acceptor structures, which facilitate the delocalization of electrons on the backbone. They found that the spin distributions and interchain interactions could lead to different spin ground states for these polymers. The low spin density and relatively uniformly distributed spin density in p(TDPP-TQ) (**15**) make it exhibit a triplet ground state. However, because of high-spin density, separately distributed spin density, and interchain antiferromagnetic spin-spin interactions in p(TDPP-BBT) (**16**), it shows the doublet state in the solid state. All these polymers showed high charge carrier mobilities and p(TDPP-TQ) exhibited record high hole and electron mobilities among all the reported high-spin organic semiconductors (Fig. 11c). In addition to the molecular structure, the arrangement of the molecules also has a great influence on the spin-spin interactions. The polymer (**17**) is treated with solvent steam-assisted slow-drying technology to enhance the intermolecular order, enabling intermolecular exchange interactions sufficient to induce and stabilize long-range spin ordering at room temperature (Fig. 8).[46] To facilitate the design of high-spin conjugated polymers, Rai *et al.* calculated the effect of atomic engineering on the spin topology.[36] Their calculations predict that the N-substituted CPDS-NBBT polymer (**18**) with large aromatic backbones showed Aufbau orbital ordering. The C (**19**), Si (**20**), and Se (**21**) substituted polymers with large quinone-type characteristics show non-Aufbau electronic configurations, which are more likely to form stable high-spin ground states. These polymers are interesting synthetic targets, but some have not been synthesized. Hutchison *et al.*[67] found that a small energy gap between the highest occupied molecular orbital (HOMO) and the lowest unoccupied molecular orbital (LUMO) in the singlet state is the best predictor for the existence of a triplet ground state, compared to previous use of a pro-quinoidal bonding character. Better use of computational means to predict molecular structure, exploring its impact on molecular spin topology through atomic engineering, molecular weight regulation, molecular arrangement,

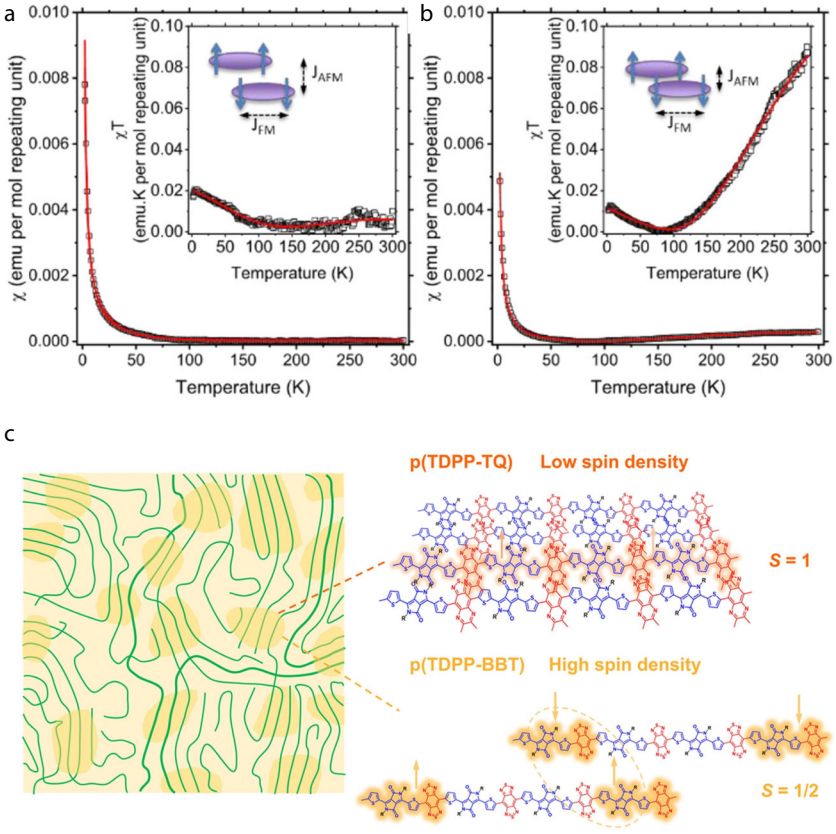

Fig. 11 SQUID measurement of (a) pBBT-2T-TT and (b) pBBT-2T-2T, fitted using a modified Bleaney-Bowers equation (red line). (Reproduced with permission from Ref. [65]; Copyright (2020), American Chemical Society.) (c) Schematic illustration of the mechanism of the different ground states of p(TDPP-TQ) and p(TDPP-BBT). The left image shows the microstructure of a typical polymer film, which contains ordered crystalline regions (highlighted in darker yellow) and amorphous regions. The right image illustrates the spin-spin interactions in the solid state. The orange shadings on the polymers indicate where the spins mostly distribute. (Reproduced with permissipon from Ref. [8]; Copyright (2022), Nature.)

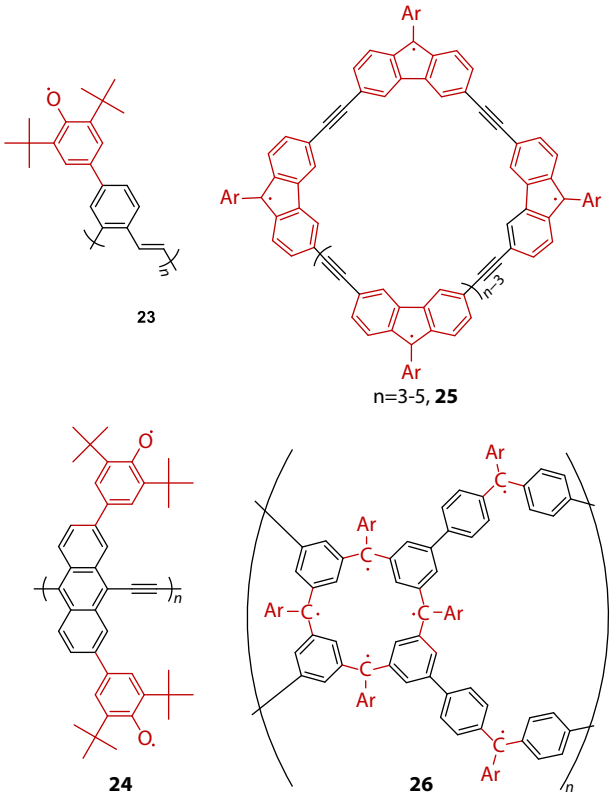

Fig. 12 Polyradical polymers or oligomers. Examples of high-spin linear polymers designed by grafting spin-containing units as pendant chains on a conjugated polymer backbone (**23** and **24**) and high-spin macrocycles (**25** and **26**).

and finding strategies to improve the spin multiplicity and magnetic order are the focus of future research. Azoulay *et al.*[7] recently developed a new strongly electron-withdrawing acceptor, 6,7,8,9-tetrachloro-[1,2,5]thiadiazolo[3,4-*b*]phenazine, and synthesized polymer **22**. The annulation and chlorination of the TQ framework facilitates a transition from the closed-shell aromatic to the high-spin quinoidal form. This is accompanied by a concurrent decrease in the bandgap, a high electron affinity, and delocalization of spin density. This arrangement influences the effective intramolecular exchange interaction (J=5.95 cm^{-1}), showcasing a stronger intramolecular coupling between spins and increasing $\Delta E_{S\text{-}T}$ by an order of magnitude compared to other high-spin conjugated polymers. The highest recorded value for $\Delta E_{S\text{-}T}$ reaches 3.40×10^{-2} kcal·mol^{-1}.

4.3 Conjugated Polymers with Polyradicals

The principle of polyradicals has been briefly introduced in section **2.2**. Appending radical units on conjugated backbones is an effective way to achieve multiple radicals. The structures of some typical polyradical polymers and oligomers are shown in Fig. 12. Tsuchida *et al.*[68] synthesized a poly(1,2-phenylenevinylene) with a 4-substituted di-*tert*-butylphenoxyl pendant group (**23**), revealing a fully conjugated backbone and long-range ferromagnetic exchange interaction among the polyphenoxyl spins. The polyphenoxyl radical, with a spin concentration of 0.4, exhibited an average spin value of 10/2. In polymer **24**,[69] the emphasis is placed on linear π-conjugated polymers that contain two pendant radicals within a single monomer unit. These radicals, forming a one-dimensional linear π-conjugated polymer, are connected through a ladder-like spin coupling network with neighbouring radical units.[69] Compared with unilaterally appended radicals with S=1,[70] it has high spin defect durability and a larger average S value of 5/2.

High-spin macrocycles have more spin-exchange paths than linear molecules but are also affected by defects and antiferromagnetic interactions. Wu *et al.*[71] found that compared to linear molecules, rigid macrocyclic structures (**25**)[72] exhibit lower doublet quadruplet energy gaps. For defect impact, Rajca *et al.*[73,74] adopted several strategies, including a cyclic structure design to provide two pathways for spin interactions and an organic spin cluster framework to minimize spin loss caused by out-of-plane twisting. The structure comprises two macrocyclic calixarene modules, one with a spin of S=2, interconnected with connecting modules having a spin of S=1/2. By incorporating a high density of macrocycles, the network aims to mitigate defects commonly encountered in such systems. In addition, the alternating connectivity of two distinct radical modules with unequal spins is expected to promote significant net S values for either ferromagnetic or antiferromagnetic coupling between the modules.

Due to the synthetic challenges of these materials, the number of polyradicals is limited. However, it is evident that the initial challenges in synthesizing polyradicals have been successfully addressed by talented polymer chemists. Moving forward, future developments will focus on designing polyradicals that exhibit ambient stability and exploring their applications in organic magnets or spintronics.

5 APPLICATIONS

5.1 OFETs

Since the initial discovery of OFETs, they have garnered significant attention in various fields such as flexible displays,[75] memory devices,[76] and sensors.[77,78] Compared with their inorganic counterparts, OFETs are highly desirable due to their excellent solution processability, low cost, and excellent flexibility. In the quest for ambipolar OFETs, which can conduct both holes and electrons, researchers have explored various single-component organic semiconductors. However, most of these ambipolar semiconductors suffer from imbalanced holes and electron mobilities. Their relatively wide band gaps of approximately 2.0 eV result in large injection barriers.[79,80] Therefore, there is a need to develop organic semiconductors with low bandgaps to achieve high-performance ambipolar OFETs.[12] Consequently, certain stable high-spin conjugated polymers with low bandgaps are well-suited to serve as ambipolar semiconductors in electronic devices. The p(TDPP-TQ) (**15**) with a triplet ground state exhibits a high electron mobility of up to 7.76±0.86 cm^2·V^{-1}·s^{-1} and a high hole mobility of up to 6.16±0.68 cm^2·V^{-1}·s^{-1} in the saturated regime (Fig. 13a). These values are among the highest values in polymer OFETs, suggesting the great potential of using high-spin polymers for ambipolar field-effect transistors.[8]

High-spin conjugated polymers also demonstrate excellent properties in n-type OFETs.[81,82] Wei *et al.*[82] introduced open-shell BBT units to the closed-shell NBDO-DTE polymer (Fig. 13b). Compared to **P1**, which only contains alternating

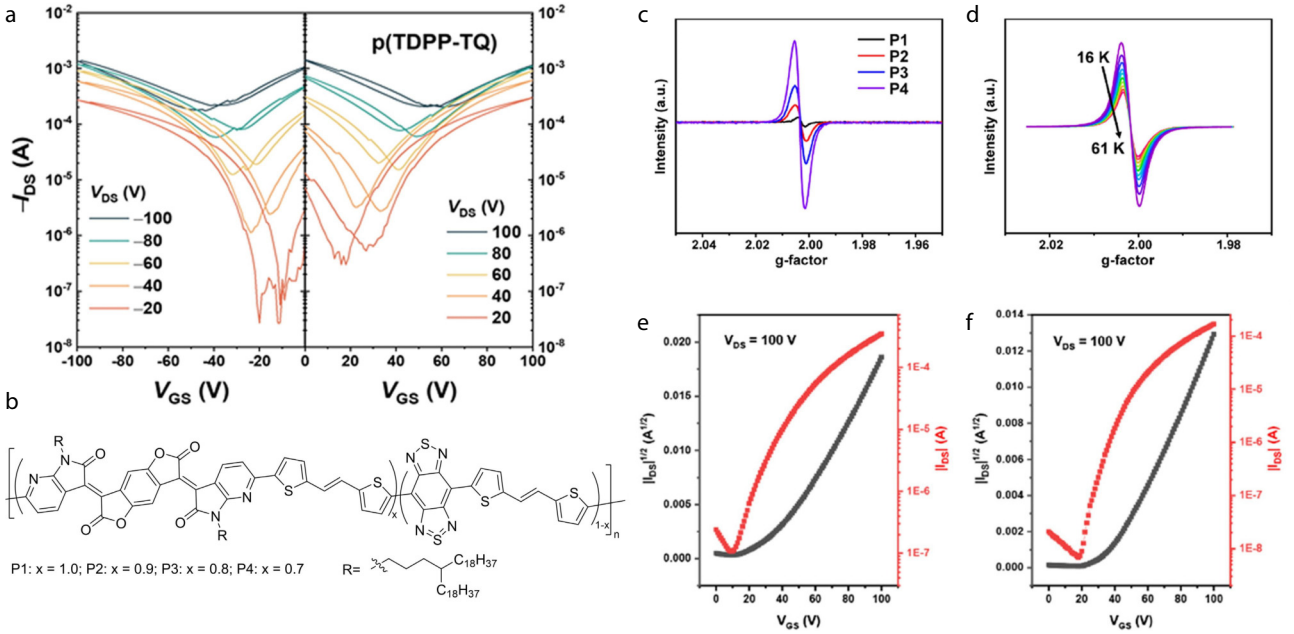

Fig. 13 (a) Typical transfer characteristics of a p(TDPP-TQ) FET device. (Reproduced with permission from Ref. [8]; Copyright (2022), Nature.) (b) Chemical structure of high mobility conjugated polymers, (c) room temperature EPR spectra of polymers **P1**–**P4**, (d) temperature-dependent EPR spectra of polymer **P4** from 61 to 16 K. Transfer curve of (e) **P1** and (f) **P2**. (Reproduced with permission from Ref. [82]; Copyright (2023), American Chemical Society.)

NBDO and DTE units, **P2**–**P4** exhibits noticeable open-shell characteristics with increased spin concentration as the BBT ratio increases (Fig. 13c). This demonstrates that the spin properties of polymer conjugated radicals can be easily adjusted by varying the BBT ratio. OFETs based on polymers **P1**–**P4** were fabricated, and they all showed unipolar n-type charge transport characteristics. Polymer **P1** exhibited the highest electron mobility of 0.64 $cm^2 \cdot V^{-1} \cdot s^{-1}$, while polymers **P2**–**P4** displayed decreased electron mobility values ranging from 0.35 $cm^2 \cdot V^{-1} \cdot s^{-1}$ to 0.12 $cm^2 \cdot V^{-1} \cdot s^{-1}$ (Figs. 13e and 13f). Microstructural investigations revealed that the decrease in mobility from **P1** to **P4** was mainly attributed to the BBT-induced molecular aggregations in the solid thin film. This work highlights that the incorporation of the open-shell moiety into the D-A polymer backbone is a promising method for developing high-spin and high-mobility polymers.

5.2 Photodetector

Polymers have several advantages when used for photodetectors. First, their tunable optoelectronic properties enable absorption across various wavelengths, facilitating tailored light absorption based on synthetic approaches. Second, the flexibility in the design and processing of polymers allows for adaptation to diverse substrates and form factors, making them highly suitable for applications in flexible electronics and wearable technologies. Third, the solution processability of polymers renders them amenable to techniques, such as printing and inkjet processing, further enhancing cost efficiency and production scalability.

However, most polymer-based photodetectors are only capable of near-infrared photodetection. High-spin polymers have a very narrow bandgap and their absorption is sufficient to extend into the long-wave infrared (LWIR) region,[10,84] which gives it the potential to be used not only for short-wave and mid-wave infrared (SWIR and MWIR) detection, but also for LWIR detection. Azoulay *et al.*[83] applied their self-designed and synthesized high-spin polymer (**14**) to infrared light detection. Variable-temperature EPR measurements show that this polymer has a $\Delta E_{S\text{-}T}$ of 9.30×10^{-3} kcal·mol^{-1} (Fig. 14a). This polymer has an extremely narrow optical bandgap (<0.10 eV). The maximum absorption wavelength of polymer thin film is 1.67 μm, covering the MWIR to LWIR range (Fig. 14b). The device showed an effective response to the SWIR, MWIR, and LWIR (Figs. 14c and 14d). The device also shows remarkable stability and its specific detectivity, an important figure of photodetector, is comparable to state-of-the-art commercial infrared detectors, especially in the far infrared region. The extremely narrow optical band gap, flexible adjustment of optoelectronic characteristics through synthesis and the ability to be processed in solution and at room temperature make them one of the most promising materials for infrared light detection.

5.3 Organic Thermoelectrics

Thermoelectric materials can realize the conversion of thermal energy and electrical energy. Compared with inorganic materials, organic thermoelectric materials have the characteristics of light weight, good flexibility, and low intrinsic thermal conductivity. The key parameters in determining the energy conversion efficiency of thermoelectric materials are conductivity (σ), Seebeck coefficient (S), and thermal conductivity (κ). This efficiency is quantified by the quality factor, ZT, which is represented by the formula $ZT = S^2\sigma\kappa^{-1}T$. In the case of polymers, their thermal conductivity is generally low. Therefore, when evaluating their thermoelectric performance, the thermoelectric power factors (PF = $S^2\sigma$) are commonly used as a performance indicator, without considering thermal conductivity. However, increasing conductivity usually accompanies an increase in charge

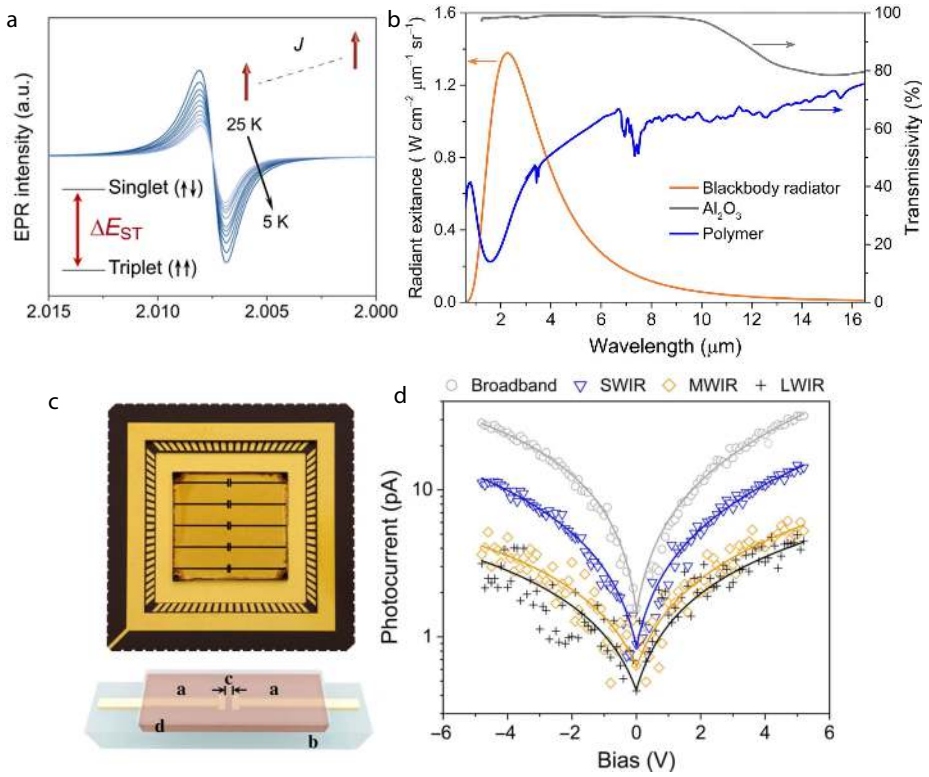

Fig. 14 (a) EPR spectra of the polymer (14) from 25 K to 5 K; (b) Transmission spectra of a thin film (blue trace); (c) Single-element photoconductive devices mounted in a ceramic leadless chip carrier. The inset shows **a** transmission lines, **b** a dielectric substrate, **c** the detector active area, and d the boundary of the polymer and dielectric encapsulant. (d) Photocurrent generated under irradiation with a 1000 °C blackbody without a spectral bandpass filter. (Reproduced with permission from Ref. [83]; Copyright (2021), the American Association for the Advancement of Science.)

carrier concentration, leading to an increase in electron scattering, which weakens the thermoelectric effect and leads to a decrease in the Seebeck coefficient. Therefore, how to improve the Seebeck coefficient without sacrificing conductivity is currently a challenge.

Tam and colleagues proposed that high thermoelectric performances can be achieved in conjugated polymers based on pro-quinoid weak acceptor structures, such as BBT.[85] Despite their amorphous nature, these polymers exhibit relatively good thermoelectric properties attributed to the formation of highly delocalized polarons. The authors further synthesized two additional polymers based on BBT, namely pBBT-2T-TT (**11**) and pBBT-2T-2T (**12**).[65] They both have a triplet ground state, DFT calculations revealed the presence of a triplet bipolaron, and pBBT-2T-TT demonstrated higher stability than pBBT-2T-2T. The Seebeck coefficient of pBBT-2T-TT was found to be higher than that of pBBT-2T-2T across all doping levels (Figs. 15a and 15b). However, field-effect measurements revealed that the mobility of pBBT-2T-TT and pBBT-2T-2T were 0.02 $cm{\cdot}V^{-1}{\cdot}s^{-1}$ and 0.25 $cm{\cdot}V^{-1}{\cdot}s^{-1}$, respectively. Thus, the carrier concentrations of pBBT-2T-TT were estimated to be approximately an order of magnitude higher than that of pBBT-2T-2T at all measured doping levels, implying a lower Seebeck coefficient. These results are opposite to the observed high Seebeck coefficient in pBBT-2T-TT. Thus the authors argue that in materials with strong electron-electron interactions, spin is expected to make a significant contribution to the Seebeck coefficient. By incorporating the pro-quinone structure into the conjugated polymer and further enhancing the Seebeck coefficient using triplet bipolarons, it is possible to achieve high electrical conductivity and simultaneously high Seebeck coefficient.

Air-stable n-type thermoelectric materials are rare. This is because conventional n-type organic thermoelectrics materials, prepared through chemical doping, tend to be highly unstable when exposed to air. Moreover, controlling doping efficiency and microstructure becomes difficult with the incorporation of external dopants. However, organic radicals present a unique case, as they can exhibit extremely small band gaps, allowing for the generation of free carriers through thermal activation. Additionally, the spin-spin interactions between radicals can enhance molecular orbital overlap, leading to increased bandwidth and improved carrier transport. Zhu *et al.*[86] reported the design and synthesis of unconventional n-type organic thermoelectrics materials based on the diradicaloids 2DQQT-S and 2DQQT-Se (Fig. 15c). These materials are demonstrated to be neutral single-component organic conductors with unprecedented air stability. Interestingly, without external n-doping, a pristine film of 2DQQT-Se exhibits remarkably high electrical conductivity of 0.29 $S{\cdot}cm^{-1}$, resulting in a power factor of 1.4 $\mu W{\cdot}m^{-1}{\cdot}K^{-2}$. Importantly, under ambient conditions, no degradation in electrical conductivity is observed for over 260 h (Fig. 15d). Azoulay *et al.*[6] discovered that the open-shell D-A copolymer, CPDT-TQ (**10**), exhibits a remarkable intrinsic p-type electrical conductivity of 8.18 $S{\cdot}cm^{-1}$, surpassing other neutral narrow bandgap con-

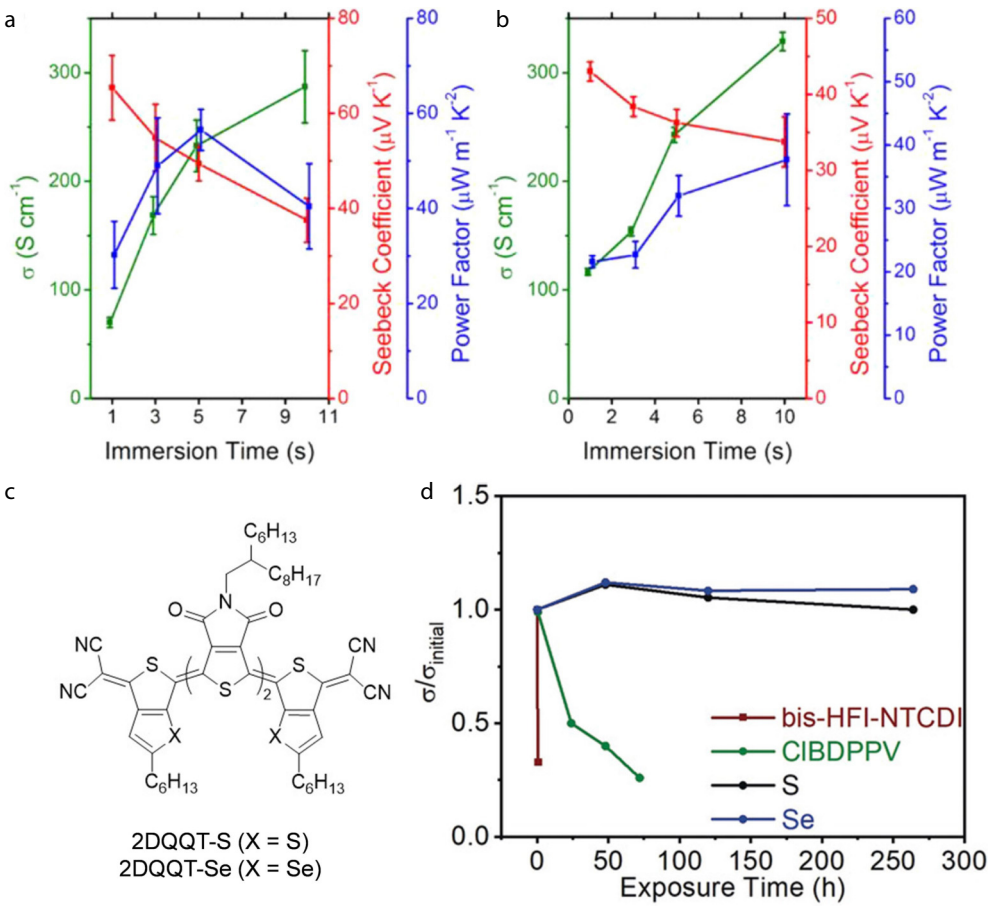

Fig. 15 Electrical conductivity, Seebeck coefficient, and power factor of (a) pBBT-2T-TT and (b) pBBT-2T-2T devices doped by $FeCl_3$. (Reproduced with permission from Ref. [65]; Copyright (2020), the American Chemical Society.) (c) Chemical structure of 2DQQT-S and 2DQQT-Se; (d) Attenuation ratios of electrical conductivity of neutral 2DQQT-S and 2DQQT-Se thin films in air with exposure time in comparison to data reported for bis-HFI-NTCDI and ClBDPPV. (Reproduced with permission from Ref. [86]; Copyright (2019), Wiley Online Library.)

jugated polymers. The open-shell conjugated polymers hold the potential for achieving high electrical conductivity under an undoped state and are promising for organic thermoelectrics applications.

5.4 Spintronics

Open-shell conjugated polymers offer a promising future in spintronic devices due to their enhanced stability,[7] high conductivity,[6] and interesting magnetic properties.[46] A study[9] reported a significant spin-lattice relaxation time of approximately 1 μs, indicating the potential for spin-polarized transport in these materials. This implies that if the magnetization axis of radicals is immobilized by an external magnetic field and spin flip scattering processes are minimized, the spins exhibit longer durations while in transit. This interplay of high conductivity, magnetism, and extended spin relaxation time is promising for spin-based electronics.

These materials also display various spin-correlated properties that can be effectively adjusted through chemical synthesis.[7,9] The paramagnetic or ferromagnetic interactions present in these radicals make them suitable as efficient spin filters, particularly for spin valve functionality. This allows the generation of pure spin current decoupled from the charge current at the device level. Utilizing open-shell materials with room temperature ferromagnetism as ferromagnetic electrodes presents an opportunity to fabricate all-organic spin valve devices. This approach addresses the conductivity mismatch issue typically encountered between metallic ferromagnetic electrodes and organic material layers. Multi-radicals, characterized by their high spin arrangement and paramagnetic properties proportional to the $S(S + 1)$ factor, hold immense potential as organic magnets. Particularly, multi-radicals derived from large cyclic polyaryl methyls have attained high-spin states, with reported maximum S values reaching 5000.[48] However, their practical application in spin electronic devices has been hindered by challenges related to stability under ambient conditions and synthesis difficulties. On the other hand, high-spin D-A conjugated polymers, though relatively less explored, offer a promising avenue for organic magnet research. These polymers exhibit stable triplet states and can be synthesized with relative simplicity. Notably, they have demonstrated a significant improvement in $\Delta E_{S\text{-}T}$, with the highest recorded value reaching 3.40×10^{-2} kcal·mol^{-1}.[7]

Recently, Azoulay *et al.*[87] found that open-shell polymers can display MR in device structures without the presence of ferromagnetic electrodes (Figs. 16a and 16b). The magnitude and sign of its MR is significantly affected by temperature. At −10 K, the device shows a giant negative MR signal of −98%

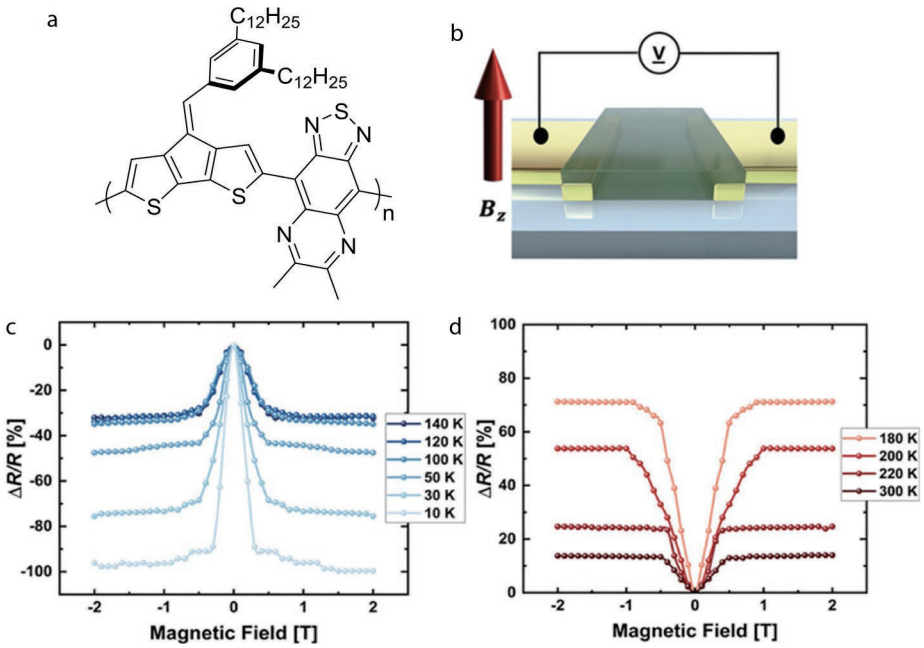

Fig. 16 (a) Chemical structure of the high-spin D-A polymer used in magnetoresistance (MR) test; (b) Thin-film device, using gold instead of ferromagnetic materials as electrodes; (c) MR curves at low temperatures; (d) MR curves at high temperatures. (Reproduced with permission from Ref. [86]; Copyright (2019), Wiley Online Library.)

(Fig. 16c). At room temperature, the device still shows a significant positive MR signal of 13.5% (Fig. 16d), which is higher than the performance of all reported organic spin valves. The superb MR properties and the specific temperature dependence exhibited by this polymer demonstrate the potential of high-spin molecules for particular applications in organic spintronics. However, the utilization of open-shell polymers in spintronic devices, such as spin valves, is still limited, and further research is needed to observe and explain their unusual properties.

6 CONCLUSIONS

In summary, our review focuses on open-shell, especially high-spin conjugated polymers, and some oligomers, covering fundamental theories, characterization methods, historical development, and applications. Currently, the field of high-spin conjugated polymers is still in its early stage compared to small molecule counterparts. However, this presents an opportunity for significant advancements in the community of radical polymer research, with a focus on elucidating the chemical structure and its correlation with the high-spin ground state. We hope that our efforts provide a suitable background and reference for inspiring further progress in this field. Furthermore, we expect more exploration of the potential of open-shell oligomers and polymers in spintronic devices and photodetectors. By delving into these areas, we could unlock the full potential of high-spin conjugated oligomers and polymers and potentially drive new advancements in spin-related technologies.

BIOGRAPHY

Ting Lei is an Assistant Professor at the School of Materials Science & Engineering, Peking University. He received his B.S. and Ph.D. degrees from Peking University in 2008 and 2013, respectively. After postdoc training at Stanford with Prof. Zhenan Bao, he joined Peking University in 2018. His current research focuses on organic/polymer functional materials, organic bioelectronics, and organic spintronics.

Conflict of Interests

The authors declare no interest conflict.

ACKNOWLEDGMENTS

This work was financially supported by Beijing Natural Science Foundation (No. JQ22006) and King Abdullah University of Science and Technology Research Funding (KRF) under Award (No. ORA-2021-CRG10-4668.4).

REFERENCES

1 Gallagher, N. M.; Olankitwanit, A.; Rajca, A. High-spin organic molecules. *J. Org. Chem.* **2015**, *80*, 1291−1298.
2 Bujak, P.; Kulszewicz-Bajer, I.; Zagorska, M.; Maurel, V.; Wielgus, I.; Pron, A. Polymers for electronics and spintronics. *Chem. Soc. Rev.* **2013**, *42*, 8895−8999.
3 Abe, M. Diradicals. *Chem. Rev.* **2013**, *113*, 7011−7088.
4 Dediu, V. A.; Hueso, L. E.; Bergenti, I.; Taliani, C. Spin routes in organic semiconductors. *Nat. Mater.* **2009**, *8*, 707−716.
5 Chen, Z. X.; Li, Y.; Huang, F. Persistent and stable organic radicals: design, synthesis, and applications. *Chem* **2021**, *7*, 288−332.
6 Ji, L.; Shi, J.; Wei, J.; Yu, T.; Huang, W. Air-stable organic radicals: new-generation materials for flexible electronics. *Adv. Mater.* **2020**, *32*, 1908015.
7 Eedugurala, N.; Steelman, M. E.; Mahalingavelar, P.; Adams, D. J.; Mayer, K. S.; Liu, C. T.; Benasco, A.; Ma, G.; Gu, X.; Bowman, M. K.;

Azoulay, J. D. Strong acceptor annulation enables control of electronic structure and spin configuration in donor-acceptor conjugated polymers. *Chem. Mater.* **2023**, *35*, 3115–3123.
8 Chen, X. X.; Li, J. T.; Fang, Y. H.; Deng, X. Y.; Wang, X. Q.; Liu, G.; Wang, Y.; Gu, X.; Jiang, S. D.; Lei, T. High-mobility semiconducting polymers with different spin ground states. *Nat. Commun.* **2022**, *13*, 2258.
9 Mayer, K. S.; Adams, D. J.; Eedugurala, N.; Lockart, M. M.; Mahalingavelar, P.; Huang, L.; Galuska, L. A.; King, E. R.; Gu, X.; Bowman, M. K.; Azoulay, J. D. Topology and ground state control in open-shell donor-acceptor conjugated polymers. *Cell Rep. Phys. Sci.* **2021**, *2*, 100467.
10 London, A. E.; Chen, H.; Sabuj, M. A.; Tropp, J.; Saghayezhian, M.; Eedugurala, N.; Zhang, B. A.; Liu, Y.; Gu, X.; Wong, B. M.; Rai, N.; Bowman, M. K.; Azoulay, J. D. A high-spin ground-state donor-acceptor conjugated polymer. *Sci. Adv.* **2019**, *5*, eaav2336.
11 Gopalakrishna, T. Y.; Zeng, W.; Lu, X.; Wu, J. From open-shell singlet diradicaloids to polyradicaloids. *Chem. Commun.* **2018**, *54*, 2186–2199.
12 Hu, X.; Wang, W.; Wang, D.; Zheng, Y. The electronic applications of stable diradicaloids: present and future. *J. Mater. Chem. C* **2018**, *6*, 11232–11242.
13 Stuyver, T.; Chen, B.; Zeng, T.; Geerlings, P.; De Proft, F.; Hoffmann, R. Do Diradicals behave like radicals. *Chem. Rev.* **2019**, *119*, 11291–11351.
14 Zhang, K.; Monteiro, M. J.; Jia, Z. Stable organic radical polymers: synthesis and applications. *Polym. Chem.* **2016**, *7*, 5589–5614.
15 Tan, Y.; Hsu, S.-N.; Tahir, H.; Dou, L.; Savoie, B. M.; Boudouris, B. W. Electronic and spintronic open-shell macromolecules, *Quo Vadis*. *J. Am. Chem. Soc.* **2022**, *144*, 626–647.
16 Ji, X.; Fang, L. Quinoidal conjugated polymers with open-shell character. *Polym. Chem.* **2021**, *12*, 1347–1361.
17 Flynn, C. R.; Michl, J. *π,π*-Biradicaloid hydrocarbons. *o*-Xylylene. Photochemical preparation from 1,4-dihydrophthalazine in rigid glass, electric spectroscopy, and calculations. *J. Am. Chem. Soc.* **1974**, *96*, 3280–3288.
18 Yamanaka, S.; Kawakami, T.; Nagao, H.; Yamaguchi, K. Effective exchange integrals for open-shell species by density-functional methods. *Chem. Phys. Lett.* **1994**, *231*, 25–33.
19 Burrezo, P. M.; Zafra, J. L.; López Navarrete, J. T.; Casado, J. Quinoidal/aromatic transformations in *π*-conjugated oligomers: vibrational raman studies on the limits of rupture for *π*-bonds. *Angew. Chem. Int. Ed.* **2017**, *56*, 2250–2259.
20 Misurkin, I. A. E.; Ovchinnikov, A. A. The electronic structures and properties of polymeric molecules with conjugated bonds. *Russ. Chem. Rev.* **1977**, *46*, 967.
21 Rajca, A.; Shiraishi, K.; Pink, M.; Rajca, S. Triplet (S = 1) ground state aminyl diradical. *J. Am. Chem. Soc.* **2007**, *129*, 7232–7233.
22 Bushby, R. J.; Taylor, N.; Williams, R. A. Ferromagnetic spin-coupling 4,4″-through metaterphenyl: models for high-spin polymers. *J. Mater. Chem.* **2007**, *17*, 955–964.
23 Wienk, M. M.; Janssen, R. A. Stable triplet-state di (cation radicals) of a *meta-para* aniline oligomer by "acid doping". *J. Am. Chem. Soc.* **1996**, *118*, 10626–10628.
24 Rajca, A., The physical organic chemistry of very high-spin polyradicals. In *Advances in Physical Organic Chemistry*, Richard, J. P., Ed. Academic Press: **2005**; Vol. 40, pp. 153–199.
25 Evangelista, F. A.; Allen, W. D.; Schaefer III, H. F. Coupling term derivation and general implementation of state-specific multireference coupled cluster theories. *J. Chem. Phys.* **2007**, *127*, 024102.
26 Carpenter, B. K.; Pittner, J.; Veis, L. Ab initio calculations on the formation and rearrangement of spiropentane. *J. Phys. Chem. A* **2009**, *113*, 10557–10563.
27 Frisch, M. e.; Trucks, G.; Schlegel, H. B.; Scuseria, G.; Robb, M.; Cheeseman, J.; Scalmani, G.; Barone, V.; Petersson, G.; Nakatsuji, H., Gaussian 16. Gaussian, Inc. Wallingford, CT: **2016**.
28 Yamaguchi, K.; Takahara, Y.; Fueno, T.; Nasu, K. Ab initio MO calculations of effective exchange integrals between transition-metal ions *via* oxygen dianions: nature of the copper-oxygen bonds and superconductivity. *Jpn. J. Appl. Phys.* **1987**, *26*, L1362.
29 Noodleman, L. Valence bond description of antiferromagnetic coupling in transition metal dimers. *J. Chem. Phys.* **1981**, *74*, 5737–5743.
30 Yamaguchi, K.; Jensen, F.; Dorigo, A.; Houk, K. A spin correction procedure for unrestricted Hartree-Fock and Møller-Plesset wavefunctions for singlet diradicals and polyradicals. *Chem. Phys. Lett.* **1988**, *149*, 537–542.
31 Kitagawa, Y.; Saito, T.; Ito, M.; Shoji, M.; Koizumi, K.; Yamanaka, S.; Kawakami, T.; Okumura, M.; Yamaguchi, K. Approximately spin-projected geometry optimization method and its application to di-chromium systems. *Chem. Phys. Lett.* **2007**, *442*, 445–450.
32 Nakano, M.; Minami, T.; Fukui, H.; Yoneda, K.; Shigeta, Y.; Kishi, R.; Champagne, B.; Botek, E. Approximate spin-projected spin-unrestricted density functional theory method: Application to the diradical character dependences of the (hyper)polarizabilities in *p*-quinodimethane models. *Chem. Phys. Lett.* **2010**, *501*, 140–145.
33 Thomas, A.; Bhanuprakash, K.; Prasad, K. M. M. K. Near infrared absorbing benzobis(thiadiazole) derivatives: computational studies point to biradical nature of the ground states. *J. Phys. Org. Chem.* **2011**, *24*, 821–832.
34 Nakano, M. Electronic structure of open-shell singlet molecules: diradical character viewpoint. *Top. Curr. Chem.* **2017**, *375*, 47.
35 Sabuj, M. A.; Huda, M. M.; Sarap, C. S.; Rai, N. Benzobisthiadiazole-based high-spin donor-acceptor conjugated polymers with localized spin distribution. *Mater. Adv.* **2021**, *2*, 2943–2955.
36 Sabuj, M. A.; Muoh, O.; Huda, M. M.; Rai, N. Non-Aufbau orbital ordering and spin density modulation in high-spin donor-acceptor conjugated polymers. *Phys. Chem. Chem. Phys.* **2022**, *24*, 23699–23711.
37 Adams, D. J.; Mayer, K. S.; Steelman, M.; Azoulay, J. D. Magnetic characterization of open-shell donor-acceptor conjugated polymers. *J. Phys. Chem. C* **2022**, *126*, 5701–5710.
38 Moss, R. A.; Platz, M. S.; Jones Jr, M. in *Reactive Intermediate Chemistry*. Wiley, **2004**.
39 Roessler, M. M.; Salvadori, E. Principles and applications of EPR spectroscopy in the chemical sciences. *Chem. Soc. Rev.* **2018**, *47*, 2534–2553.
40 Bleaney, B.; Bowers, K. Anomalous paramagnetism of copper acetate. *Proc. L., Seri. A* **1952**, *214*, 451–465.
41 Jenks, W.; Sadeghi, S.; Wikswo Jr, J. P. SQUIDs for nondestructive evaluation. *J. Phys. D: Appl. Phys.* **1997**, *30*, 293.
42 Buchner, M.; Höfler, K.; Henne, B.; Ney, V.; Ney, A. Tutorial: basic principles, limits of detection, and pitfalls of highly sensitive SQUID magnetometry for nanomagnetism and spintronics. *J. Appl. Phys.* **2018**, *124*, 161101.
43 Bain, G. A.; Berry, J. F. Diamagnetic corrections and Pascal's constants. *J. Chem. Edu.* **2008**, *85*, 532.
44 Dressler, J. J.; Valdivia, A. C.; Kishi, R.; Rudebusch, G. E.; Ventura, A. M.; Chastain, B. E.; Gómez-García, C. J.; Zakharov, L. N.; Nakano, M.; Casado, J. Diindenoanthracene diradicaloids enable rational, incremental tuning of their singlet-triplet energy gaps. *Chem* **2020**, *6*, 1353–1368.
45 Cullity, B. D.; Graham, C. D. in *Introduction to magnetic materials*. John Wiley & Sons: **2011**.
46 Steelman, M. E.; Adams, D. J.; Mayer, K. S.; Mahalingavelar, P.; Liu, C. T.; Eedugurala, N.; Lockart, M.; Wang, Y.; Gu, X.; Bowman, M. K.; Azoulay, J. D. Magnetic ordering in a high-spin donor-acceptor conjugated polymer. *Adv. Mater.* **2022**, *34*, 2206161.
47 Darby, M. I. Tables of the Brillouin function and of the related function for the spontaneous magnetization. *Br. J. Appl. Phys.* **1967**, *18*, 1415.
48 Rajca, A.; Wongsriratanakul, J.; Rajca, S. Magnetic ordering in an

organic polymer. *Science* **2001**, *294*, 1503–1505.
49 Li, Y.; Li, L.; Wu, Y.; Li, Y. A review on the origin of synthetic metal radical: singlet open-shell radical ground state. *J. Phys. Chem. C* **2017**, *121*, 8579–8588.
50 Thiele, J.; Balhorn, H. Ueber einen chinoïden Kohlenwasserstoff. *Ber. Dtsch. Chem. Ges.* **1904**, *37*, 1463–1470.
51 Tschitschibabin, A. E. Über einige phenylierte Derivate des p,p-Ditolyls. *Ber. Dtsch. Chem. Ges*. **1907**, *40*, 1810–1819.
52 Melby, L.; Harder, R.; Hertler, W.; Mahler, W.; Benson, R.; Mochel, W. Substituted quinodimethans. II. Anion-radical derivatives and complexes of 7,7,8,8-tetracyanoquinodimethan. *J. Am. Chem. Soc.* **1962**, *84*, 3374–3387.
53 Maxfield, M.; Bloch, A. N.; Cowan, D. O. Large electron acceptors for molecular metals: 13,13,14,14-tetracyano-4,5,9,10-tetrahydro-2,7-pyrenoquinodimethane (TCNTP) anions of 13,13,14,14-tetracyano-2,7-pyrenoquinodimethane (TCNP). *J. Org. Chem.* **1985**, *50*, 1789–1796.
54 Zeng, Z.; Ishida, M.; Zafra, J. L.; Zhu, X.; Sung, Y. M.; Bao, N.; Webster, R. D.; Lee, B. S.; Li, R. W.; Zeng, W. Pushing extended *p*-quinodimethanes to the limit: stable tetracyano-oligo (*N*-annulated perylene) quinodimethanes with tunable ground states. *J. Am. Chem. Soc.* **2013**, *135*, 6363–6371.
55 Yui, K.; Aso, Y.; Otsubo, T.; Ogura, F. Novel electron acceptors bearing a heteroquinonoid system. i. Synthesis and conductive complexes of 5,5′-bis(dicyanomethylene)-5,5′-dihydro-Δ2,2′-bithiophene and related compounds. *Bull. Chem. Soc. Jpn.* **1989**, *62*, 1539–1546.
56 Takahashi, T.; Matsuoka, K. I.; Takimiya, K.; Otsubo, T.; Aso, Y. Extensive quinoidal oligothiophenes with dicyanomethylene groups at terminal positions as highly amphoteric redox molecules. *J. Am. Chem. Soc.* **2005**, *127*, 8928–8929.
57 Ponce Ortiz, R.; Casado, J.; Hernández, V.; López Navarrete, J. T.; Viruela, P. M.; Ortí, E.; Takimiya, K.; Otsubo, T. On the biradicaloid nature of long quinoidal oligothiophenes: experimental evidence guided by theoretical studies. *Angew. Chem.* **2007**, *119*, 9215–9219.
58 Slota, M.; Keerthi, A.; Myers, W. K.; Tretyakov, E.; Baumgarten, M.; Ardavan, A.; Sadeghi, H.; Lambert, C. J.; Narita, A.; Müllen, K.; Bogani, L. Magnetic edge states and coherent manipulation of graphene nanoribbons. *Nature* **2018**, *557*, 691–695.
59 Zeng, W.; Phan, H.; Herng, T. S.; Gopalakrishna, T. Y.; Aratani, N.; Zeng, Z.; Yamada, H.; Ding, J.; Wu, J. Rylene ribbons with unusual diradical character. *Chem* **2017**, *2*, 81–92.
60 Guo, J.; Tian, X.; Wang, Y.; Dou, C. Progress of indeno-type organic diradicaloids. *Chem. Res. Chin. Univ.* **2023**, *39*, 161–169.
61 Hayashi, H.; Barker, J. E.; Cárdenas Valdivia, A.; Kishi, R.; MacMillan, S. N.; Gómez-García, C. J.; Miyauchi, H.; Nakamura, Y.; Nakano, M.; Kato, S. I.; Haley, M. M.; Casado, J. Monoradicals and diradicals of dibenzofluoreno[3,2-*b*]fluorene isomers: mechanisms of electronic delocalization. *J. Am. Chem. Soc.* **2020**, *142*, 20444–20455.
62 Chen, Z.; Li, W.; Zhang, Y.; Wang, Z.; Zhu, W.; Zeng, M.; Li, Y. Aggregation-induced radical of donor-acceptor organic semiconductors. *J. Phys. Chem. Lett.* **2021**, *12*, 9783–9790.
63 Liu, Y.; Phan, H.; Herng, T. S.; Gopalakrishna, T. Y.; Ding, J.; Wu, J. Toward benzobis(thiadiazole)-based diradicaloids. *Chem. Asian J.* **2017**, *12*, 2177–2182.
64 Chen, Z.; Li, W.; Sabuj, M. A.; Li, Y.; Zhu, W.; Zeng, M.; Sarap, C. S.; Huda, M. M.; Qiao, X.; Peng, X.; Ma, D.; Ma, Y.; Rai, N.; Huang, F. Evolution of the electronic structure in open-shell donor-acceptor organic semiconductors. *Nat. Commun.* **2021**, *12*, 5889.
65 Tam, T. L. D.; Wu, G.; Chien, S. W.; Lim, S. F. V.; Yang, S. W.; Xu, J. High spin pro-quinoid benzo[1,2-*c*;4,5-*c*′]bisthiadiazole conjugated polymers for high-performance solution-processable polymer thermoelectrics. *ACS Mater. Lett.* **2020**, *2*, 147–152.
66 Yuen, J. D.; Wang, M.; Fan, J.; Sheberla, D.; Kemei, M.; Banerji, N.; Scarongella, M.; Valouch, S.; Pho, T.; Kumar, R.; Chesnut, E. C.; Bendikov, M.; Wudl, F. Importance of unpaired electrons in organic electronics. *J. Polym. Sci., Part A: Polym. Chem.* **2015**, *53*, 287–293.
67 Abarbanel, O. D.; Rozon, J.; Hutchison, G. R. Strategies for computer-aided discovery of novel open-shell polymers. *J. Phys. Chem. Lett.* **2022**, *13*, 2158–2164.
68 Nishide, H.; Ozawa, T.; Miyasaka, M.; Tsuchida, E. A nanometer-sized high-spin polyradical: poly(4-phenoxyl-1,2-phenylenevinylene) planarily extended in a non-kekulé fashion and its magnetic force microscopic images. *J. Am. Chem. Soc.* **2001**, *123*, 5942–5946.
69 Kaneko, T.; Makino, T.; Miyaji, H.; Teraguchi, M.; Aoki, T.; Miyasaka, M.; Nishide, H. Ladderlike ferromagnetic spin coupling network on a *π*-conjugated pendant polyradical. *J. Am. Chem. Soc.* **2003**, *125*, 3554–3557.
70 Kaneko, T.; Matsubara, T.; Aoki, T. Synthesis of a pendant polyradical with a new *π*-conjugated polymer backbone containing an anthracene skeleton and its ferromagnetic spin coupling. *Chem. Mater.* **2002**, *14*, 3898–3906.
71 Lu, X.; Lee, S.; Kim, J. O.; Gopalakrishna, T. Y.; Phan, H.; Herng, T. S.; Lim, Z.; Zeng, Z.; Ding, J.; Kim, D.; Wu, J. Stable 3,6-linked fluorenyl radical oligomers with intramolecular antiferromagnetic coupling and polyradical characters. *J. Am. Chem. Soc.* **2016**, *138*, 13048–13058.
72 Lu, X.; Lee, S.; Hong, Y.; Phan, H.; Gopalakrishna, T. Y.; Herng, T. S.; Tanaka, T.; Sandoval-Salinas, M. E.; Zeng, W.; Ding, J.; Casanova, D.; Osuka, A.; Kim, D.; Wu, J. Fluorenyl based macrocyclic polyradicaloids. *J. Am. Chem. Soc.* **2017**, *139*, 13173–13183.
73 Rajca, A.; Wongsriratanakul, J.; Rajca, S. Organic spin clusters: macrocyclic-macrocyclic polyarylmethyl polyradicals with very high spin $S = 5–13$. *J. Am. Chem. Soc.* **2004**, *126*, 6608–6626.
74 Rajca, A.; Rajca, S.; Wongsriratanakul, J. Very high-spin organic polymer: *π*-conjugated hydrocarbon network with average spin of $S \geq 40$. *J. Am. Chem. Soc.* **1999**, *121*, 6308–6309.
75 Sirringhaus, H. 25th Anniversary article: organic field-effect transistors: the path beyond amorphous silicon. *Adv. Mater.* **2014**, *26*, 1319–1335.
76 Chou, Y. H.; Chang, H. C.; Liu, C. L.; Chen, W. C. Polymeric charge storage electrets for non-volatile organic field effect transistor memory devices. *Polym. Chem.* **2015**, *6*, 341–352.
77 Knopfmacher, O.; Hammock, M. L.; Appleton, A. L.; Schwartz, G.; Mei, J.; Lei, T.; Pei, J.; Bao, Z. Highly stable organic polymer field-effect transistor sensor for selective detection in the marine environment. *Nat. Commun.* **2014**, *5*, 2954.
78 Sokolov, A. N.; Tee, B. C.; Bettinger, C. J.; Tok, J. B. H.; Bao, Z. Chemical and engineering approaches to enable organic field-effect transistors for electronic skin applications. *Acc. Chem. Res.* **2012**, *45*, 361–371.
79 Singh, T. B.; Meghdadi, F.; Günes, S.; Marjanovic, N.; Horowitz, G.; Lang, P.; Bauer, S.; Sariciftci, N. S. High-performance ambipolar pentacene organic field-effect transistors on poly(vinyl alcohol) organic gate dielectric. *Adv. Mater.* **2005**, *17*, 2315–2320.
80 Anthopoulos, T. D.; Setayesh, S.; Smits, E.; Cölle, M.; Cantatore, E.; de Boer, B.; Blom, P. W. M.; de Leeuw, D. M. Air-stable complementary-like circuits based on organic ambipolar transistors. *Adv. Mater.* **2006**, *18*, 1900–1904.
81 Kim, Y.; Yang, D.; Kim, Y. J.; Jung, E.; Park, J. J.; Choi, Y.; Kim, Y.; Mathur, S.; Kim, D. Y.. Azaquinoid-based high spin open-shell conjugated polymer for n-type organic field-effect transistors. *Adv. Mater. Interfaces* **2023**, *10*, 2201205.
82 Wei, X.; Pan, Y.; Zhang, W.; Zhou, Y.; Li, H.; Wang, L.; Yu, G. Incorporation of the benzobisthiadiazole unit leads to open-shell conjugated polymers with n-type charge transport properties. *Macromolecules* **2023**, *56*, 2980–2989.
83 Vella, J. H.; Huang, L.; Eedugurala, N.; Mayer, K. S.; Ng, T. N.; Azoulay, J. D. Broadband infrared photodetection using a narrow bandgap conjugated polymer. *Sci. Adv.* **2021**, *7*, eabg2418.

https://doi.org/10.1007/s10118-024-3087-7

84 Huang, L.; Eedugurala, N.; Benasco, A.; Zhang, S.; Mayer, K. S.; Adams, D. J.; Fowler, B.; Lockart, M. M.; Saghayezhian, M.; Tahir, H.; King, E. R.; Morgan, S.; Bowman, M. K.; Gu, X.; Azoulay, J. D. Open-shell donor-acceptor conjugated polymers with high electrical conductivity. *Adv. Funct. Mater.* **2020**, *30*, 1909805.
85 Tam, T. L. D.; Ng, C. K.; Lim, S. L.; Yildirim, E.; Ko, J.; Leong, W. L.; Yang, S.-W.; Xu, J. Proquinoidal-conjugated polymer as an effective strategy for the enhancement of electrical conductivity and thermoelectric properties. *Chem. Mater.* **2019**, *31*, 8543–8550.
86 Yuan, D.; Guo, Y.; Zeng, Y.; Fan, Q.; Wang, J.; Yi, Y.; Zhu, X. Air-stable n-type thermoelectric materials enabled by organic diradicaloids. *Angew. Chem. Int. Ed.* **2019**, *58*, 4958–4962.
87 Tahir, H.; Eedugurala, N.; Hsu, S. N.; Mahalingavelar, P.; Savoie, B. M.; Boudouris, B. W.; Azoulay, J. D. Large room-temperature magnetoresistance in a high-spin donor-acceptor conjugated polymer. *Adv. Mater.* **2023**, *36*, 2306389.

https://doi.org/10.1007/s10118-024-3087-7